Modeling Shortest Paths in Polymeric Networks using Spatial Branching Processes

Zhenyuan Zhang[a,1], Shaswat Mohanty[b,1], Jose Blanchet[c,*], Wei Cai[b,*]

[a]*Department of Mathematics, Stanford University, CA 94305-4040, USA*
[b]*Department of Mechanical Engineering, Stanford University, CA 94305-4040, USA*
[c]*Department of Management Science and Engineering, Stanford University, CA 94305-4040, USA*

Abstract

Recent studies have established a connection between the macroscopic mechanical response of polymeric materials and the statistics of the shortest path (SP) length between distant nodes in the polymer network. Since these statistics can be costly to compute and difficult to study theoretically, we introduce a branching random walk (BRW) model to describe the SP statistics from the coarse-grained molecular dynamics (CGMD) simulations of polymer networks. We postulate that the first passage time (FPT) of the BRW to a given termination site can be used to approximate the statistics of the SP between distant nodes in the polymer network. We develop a theoretical framework for studying the FPT of spatial branching processes and obtain an analytical expression for estimating the FPT distribution as a function of the cross-link density. We demonstrate by extensive numerical calculations that the distribution of the FPT of the BRW model agrees well with the SP distribution from the CGMD simulations. The theoretical estimate and the corresponding numerical implementations of BRW provide an efficient way of approximating the SP distribution in a polymer network. Our results have the physical meaning that by accounting for the realistic topology of polymer networks, extensive bond-breaking is expected to occur at a much smaller stretch than that expected from idealized models assuming periodic network structures. Our work presents the first analysis of polymer networks as a BRW and sets the framework for developing a generalizable spatial branching model for studying the macroscopic evolution of polymeric systems.

Keywords: Branching Brownian Motion, Branching Random Walk, Coarse-Grained Molecular Dynamics, First Passage Time, Polymer Network, Shortest Path Statistics, 8-chain model

*Corresponding author
[1]Equal contribution

1. Introduction

Polymers play a vital role in technology and products of daily use due to their wide-ranging utility. An important class of polymers is elastomers [1–3], which are rubber-like materials that exhibit an elastic response even under high strains. The elastic and hyperelastic behavior of these materials has been modeled across various length scales from the continuum [4, 5] down to the microstructural scale [6, 7]. However, their inelastic response due to the bond-breaking events is not well understood. Recently, we have shown that network analysis can be applied to coarse-grained molecular dynamics (CGMD) models to explain the experimentally observed stress-strain hysteresis [8] in elastomers by identifying the shortest path length between distant nodes as the governing microstructural parameter [9, 10].

The CGMD model comprises a large number of beads (to represent the polymer chains and cross-linking ligands), and the preparation of these systems until they reach equilibrium is a time-consuming process. Given that the macroscopic response is shown to strongly depend on the network statistics of the shortest paths, there is an incentive to replace expensive CGMD simulations with a probabilistic model that represents the polymer network. Representing polymer networks as random walks and evaluating their response under load has a long tradition in polymer theory [11]. However, the focus of these studies has been on the conformation of individual polymer chains, and not so much on the statistics involving the whole network topology, in our case, the shortest path distribution.

In this paper, we discuss the statistical properties of the shortest path length (SPL, abbreviated as SP) distribution between far-away nodes with polymer networks modeled as branching random walks (BRWs). The SP in the polymer network corresponds to the first passage time (FPT) of the BRW, i.e., the time taken for the BRW to reach a prescribed sink or halt criterion. Roughly speaking, in a BRW we start from one particle at the origin and each existing particle independently performs a random walk until it (randomly) branches into more particles,[2] according to a certain branching rate. Here, the branching rate in the BRW corresponds to the cross-link density in the polymeric system, and the random walk paths correspond to the polymer chains. We also establish theoretical predictions of the FPT of the BRW. We show that the SP distributions predicted from the CGMD simulations are consistent with the numerical implementation of the BRW model, as well as with theoretical BRW estimates. In particular, our theoretical results on the FPT of the BRW provide explicit formulas that predict the mean SP from the CGMD network given the cross-link density. In addition, we show that in the long-distance limit, the fluctuation of the FPT is asymptotically much lower than its expected value, a property validated by CGMD simulations.

Analyzing the extremal behavior of spatial branching processes is an active area of

[2]The BRW describes the positions of *particles* evolving in time. We do not intend this evolution to represent the time evolution of the CGMD network. Following the tradition in polymer theory, we represent typical polymer chains as random walks, but we explicitly model the cross-link topology by the branching mechanism.

recent research in probability theory. Such processes include BRW and its continuous-time sibling, the branching Brownian motion (BBM), as well as various extensions. The literature has focused mostly on the asymptotics of the maximum and the limit behavior near the maximum; see the works [12–15] for the case of one-dimensional BRW and [16–20] for one-dimensional BBM, among others. Here we are interested in branching structures in higher (e.g. 3) dimensions (that represent real physical systems), where we mention the recent studies of [21–24] on the location of the maximum norm. Nevertheless, we are not aware of the results regarding the FPT of spatial branching structures in general dimensions.[3] Our work provides a necessary first step towards understanding the limit behavior of the FPT beyond dimension one.

Our theoretical results on the FPT of spatial branching processes provide explicit formulas that predict the mean SP from the CGMD network given the cross-link density. The mean SP of the polymeric system denotes how stretched the average load-bearing polymer chain in the system is, thereby serving as an important microstructural parameter that can describe the macroscopic response of the material. The mean SP determines the maximum stretch that can be applied to the polymer before significant bond-breaking events occur, thus providing a measure of the stretchability before appreciable strain-induced damage. Our theoretical estimates from the spatial branching processes show that the stretchability of polymer before bond breaking is much smaller than estimates based on idealized, periodically repeating, network topologies, such as in the eight-chain model [6]. Our findings demonstrate that spatial branching processes are remarkably successful in capturing the SP statistics of polymer networks and are highly promising in revealing the microstructural origin of the mechanical properties of polymeric materials.

The rest of the paper is structured as follows. In Section 2, we discuss the CGMD model that is used to obtain the equilibrated network in which the reference SP calculations are carried out. In addition, we present a high-level description of our numerical BRW model and some of its extensions. In Section 3, we numerically analyze the FPT of our spatial branching models and present the consistency with the SP distribution of the CGMD network. In Section 4, we present analytic expressions for the FPT of the BRW models. Section 5 concludes the article with discussions on several future research directions.

2. Numerical methods

This section provides a high-level overview of the connections between the CGMD model of polymers and BRW processes. In particular, we compare the basic features of the CGMD and their analogs in the BRW model, which motivate extensions of the classical BRW model. We also discuss an efficient numerical algorithm for computing the FPT of the BRW and its extensions.

[3] By continuity of the trajectories, it is not hard to show that the FPT in dimension one is precisely the inversion of the maximum.

2.1. Coarse-grained molecular dynamics

We use the bead-spring (Kremer-Grest) model [7] for a CGMD representation of the polymeric system. The simulations were carried out using LAMMPS [25] where the initial configuration of $N_c = 500$ chains comprising $l_c = 500$ beads each (250,000 beads in total) is generated as a self-avoiding random walk. The simulation cell is a cube of length $\approx 98.2\,\text{nm}$ and is subjected to periodic boundary conditions in all directions. The non-bonded pair interactions between beads are modeled by a Lennard-Jones (LJ) potential, U_{LJ}, with

$$U_{\text{LJ}}(r) = 4\varepsilon \left[\left(\frac{\sigma}{r}\right)^{12} - \left(\frac{\sigma}{r}\right)^{6} \right],$$

where $\sigma = 15\,\text{Å}$ is the size of the bead, $\varepsilon = 2.5$ kJ/mol is depth of the energy well and r is the inter-bead distance. All distances in this paper will be discussed in terms of σ. As a result, the non-dimensional bead size will be $\sigma = 1$. The neighboring interactions between beads on the polymer backbone are modeled using the finite extensible (FENE) bond potential [7], U_{FENE}, allowing for the incorporation of the non-linear elastic response of the polymer backbone, with

$$U_{\text{FENE}}(r) = -k \left(\frac{R_0^2}{2}\right) \ln \left[1 - \left(\frac{r}{R_0}\right)^2 \right],$$

where $k = 30\,\varepsilon/\sigma^2$ is the bond stiffness, and $R_0 = 1.5\,a$ is the extensibility limit. The initial configuration is equilibrated using the two-step procedure [26] to obtain the equilibrated *baseline configuration* (i.e. a polymer melt), which is then modified to incorporate cross-links.

Once the baseline configuration is well equilibrated, the candidate bonding beads are identified by choosing distinct bead pairs that lie within a cutoff distance of $r_c < 1.15\,\sigma$. We then randomly choose from the set of candidate bead pairs and assign an irreversible cross-link between the chosen pairs. To model the irreversible cross-links, we use a quartic bond potential U_{Q} [27], defined by

$$U_{\text{Q}}(r) = \begin{cases} K(r - R_c)^2(r - R_c - B_1)(r - R_c - B_2) + U_0 & \text{for } r \leqslant R_c, \\ 0 & \text{for } r > R_c. \end{cases}$$

Here $K = 1200\,\varepsilon/a^4$ is the bond stiffness, $B_1 = -0.55\,a$, $B_2 = 0.95\,a$, $U_0 = 34.6878\,\varepsilon$, and $R_c = 1.3\,a$ is the cutoff distance beyond which the quartic bond is considered broken (and cannot be formed again). This procedure is identical to the preparation of a single-network (SN) elastomer model in [9].

2.2. Network analysis

We describe the polymer network from the CGMD simulation cell by only considering the cross-linking beads in the system. Cross-linking beads that are connected to each other along the backbone of the polymer chain are denoted by a graph edge with a weight equal to the number of bonds between them. Furthermore, we also define an

edge between the pair of cross-linking nodes that are involved in forming a cross-link, with an edge weight of 1. Further details regarding the network representation and SP calculation can be found in [9]. For each node i, we find a destination node j that is closest to the point offset from node i by q_x in the x-direction and compute the shortest path length (SP) connecting nodes i and j. The non-local microstructural measure of the SP has the advantage of being independent of chain conformational fluctuations and they only depend on the network connectivity, as a result evolving only as a function of the evolution of the polymer connectivity network. We compute the SPs starting from all nodes in the polymer network using Dijkstra's algorithm [28], giving rise to a distribution. We are interested in how this distribution depends on the choice of distance q_x, where $0 < q_x \leqslant L_x$ and L_x is the periodic length of the simulation cell in the x-direction. Note that when $q_x = L_x$, node j is the periodic image of node i and the simulation box is replicated in the x-direction for the SP calculation, as shown in Figure 1(a).

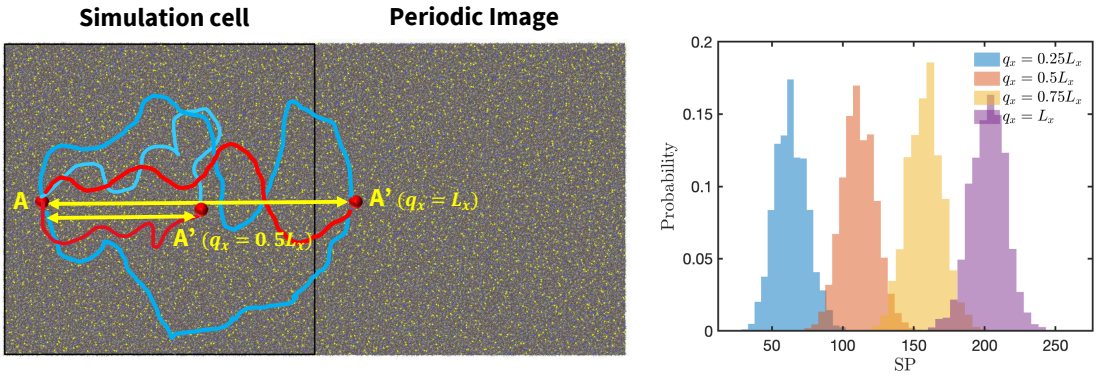

(a) (b)

Figure 1: (a) The SP between A and the destination node A' (shown in red) separated by different distances q_x in the CGMD simulation cell (the longer paths are shown in blue).[4] (b) The SP distributions for all nodes at different values of q_x, where $L_x = 65.5\,\sigma$.

As an example, Figure 1(b) plots the SP histogram from the CGMD simulation cell at offset distances of $q_x = 0.25L_x$, $0.5L_x$, $0.75L_x$, L_x, respectively. The SP distribution appears to have a mean that increases linearly with q_x, and a standard deviation that is insensitive to q_x. There does not exist any theory or analysis in the literature that explains this behavior. Furthermore, brute-force computation of the SP distribution is time-consuming, requiring lengthy equilibration of the CGMD network followed by SP calculation for all network nodes. These limitations provide the motivation to obtain theoretical estimates of the SP statistics based on analytically tractable models.

[4]Note that if the offset distance q_x is equal to the simulation cell size L_x, we are guaranteed to find the destination node at the exact distance since it is the periodic image of the source node. However, for any other value of q_x, we search for the nearest node as the destination node.

2.3. Branching random walk

In the classical setting, a (discrete-time) branching random walk (BRW) in $\mathbb{R}^d$ describes a stochastic process indexed by $n = 0, 1, 2, \ldots$, where starting from a single particle at $\mathbf{0} \in \mathbb{R}^d$ at time $n = 0$, each particle performs a standard random walk (e.g., with independent increments that are uniformly distributed on the sphere $\mathbb{S}^{d-1} = \{\mathbf{x} \in \mathbb{R}^d \mid \|\mathbf{x}\| = 1\}$),[5] but randomly reproduces particles at each time step, independently from each other and from their common ancestor(s). The trajectories of the particles form a (possibly infinite) tree in $\mathbb{R}^d$. We will be mostly interested in the physical space of dimension $d = 3$.

At first sight, there are a few reasons that motivate why the BRW may serve as a good proxy for the SP statistics of polymer networks:

- It is well known that the equilibrium configuration of single chains in a polymer melt can be well described by a random walk [11, 29, 30]. In our CGMD model, the cross-links are added into well-equilibrated polymer melt, and hence we expect the path obtained by traversing along the backbone of the polymer network to be also well described by a random walk. While a cross-link in the polymer network joins two polymer chains together, this can be modeled by extending the random walk to allow a branching process where one walker becomes three walkers.

- The BRW has a mathematically rich and relatively tractable structure. The extremal behavior of the BRW is a well-studied subject in probability theory. For example, in dimension $d = 1$, a precise asymptotic of the largest displacement of the BRW particles is well known [12], and the limit behavior near the frontier has been fully characterized [15, 19].

- The BRW allows enough freedom in the choice of parameters, such as the random walk step-size distribution and the branching rate. These parameters may be chosen appropriately so that the statistics of the FPT in the BRW model agree well with that of the SP in the CGMD model of the polymer network.

The BRW provides an alternative point of view to the polymer network. As shown in Figure 2(a), the traversal along the backbone of the polymer (starting from node A) is the equivalent of a random walk path and the point of cross-linking can be thought of as a branching event, where the path splits into *three* paths: (i) continuation of the polymer backbone ($A \to A''$), and (ii) two parts of another polymer chain ($B \to B''$). We would like to point out that what the branching random walk model aims to mimic is the part of the polymer network that emanates from a single node, rather than the entire network. Cross-links in polymers typically bind monomers (on chains) that are physically close to each other, and the occurrence of the cross-linking events in space can often be described by a Poisson process. In the BRW model, we incorporate the cross-linking effect by allowing an effective branching rate of $\widetilde{\kappa}$. However, in certain

[5] Throughout this paper, we use the Euclidean (ℓ_2) norm.

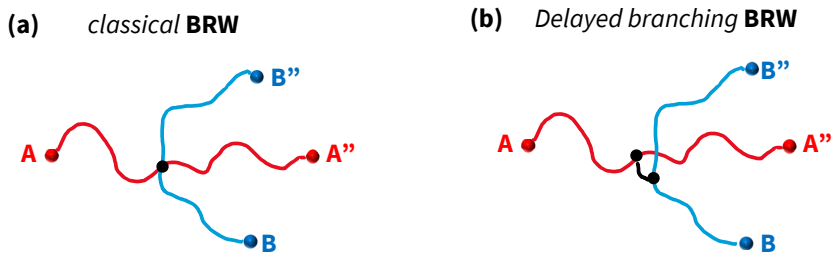

Figure 2: BRW tree representations in the (a) classical and the (b) delayed branching regimes.

polymer systems, cross-links can be controlled to occur only at specific sites, e.g. those evenly distributed along the polymer backbone [31]. This could be modeled using deterministic branching events, that occur once every $1/\widetilde{\kappa}$ steps. In this paper, we restrict our discussion to the polymer systems where the cross-linking follows a Poisson process, where $\widetilde{\kappa}$ is obtained from the CGMD simulation cell (see below).

BRW algorithm. The BRW is initialized at the origin as a single path with the branching probability $\widetilde{\kappa}$ at every time step into three paths. Every subsequent branched child has the same branching likelihood at every time step. The jumps are of a fixed constant length σ, corresponding to the bead size in the CGMD simulation cell. Similar to the SP calculations in the CGMD model, we terminate the BRW (and record FPT) as soon as any of the random walkers hits within a sphere of radius $R_c = \sigma$ centered at $(q_x, 0, 0)$. Given that each step corresponds to a unit of time, we can calculate the FPT (equivalent to the SP) for a BRW. Here, the radius for the termination region specifies the maximum deviation from the destination at an offset distance of q_x from the origin, similar to the SP analysis in the CGMD model.[6]

Branching rate estimation. In the case of the polymer network modeled in the CGMD simulation, the cross-link formation between proximal inter-polymer sites mimics a Poisson point process. We can track all the inter-cross-link distances along the polymer backbone, denoted by the variable x_b. The survival function ($1-\mathrm{CDF}(x_b)$) of the histogram of x_b approximates the exponential decay $x \mapsto \exp(-\kappa_a x)$. Here, the exponent κ_a is the arrival rate for a Poisson process. In our estimation of the branching rate $\widetilde{\kappa} = \kappa_a$, we will obtain the κ_a from the cotangent of the logarithm of the survival function of the x_b distribution, given by $1-\mathrm{CDF}(x_b)$.

Numerical implementation. Tracking all the branched paths (children) of the BRW tree is memory intensive. To circumvent this difficulty, in the numerical representation of the BRW model, we purge the tracks that are farthest away from the termination point. In our implementation, we fix a large number $p_c = 9000$ and include a *path purging* step, where once the number n_p of tracked paths exceeds p_c we trim down the number of paths to $p_c/3$. Our numerical results (in Appendix B) support the expectation that

[6]The quality of our models are not sensitive to the choice of radius R_c; any value within the same order of magnitude would give qualitatively the same result.

path purging does not noticeably affect FPT calculations. There is also theoretical support for this expectation, e.g. by Theorem 3.1 of [23] and the discussions therein.

2.4. Extensions of the classical branching random walk model

A closer examination of the classical BRW model reveals the following features of the CGMD model of the polymer network that have not yet been taken into account.

- The length of the cross-link is neglected. For the classical BRW model, the cross-links are assumed to have zero length and are not taken into account when computing the SP statistics. On the other hand, each cross-link in the CGMD model has a non-zero length and is counted towards the SP.
- The polymer chains (before cross-linking) have a finite length of $l_c = 500$ beads each in the CGMD model, and hence we would expect a termination rate for the corresponding BRW model for consistency.
- There is a nontrivial correlation between neighboring link vectors on a polymer chain in the CGMD network. The classical BRW model fails to incorporate such correlation effects since its increments are independent.

For these reasons, we introduce the following important extensions of the classical BRW model that more accurately represent the network in our CGMD configurations.

Delayed branching regime. We introduce a two-step branching regime. Instead of each random walker immediately branching into three walkers, each branching event now consists of two sub-events, as shown in Figure 2(b). First, the walker branches into two walkers; the trajectory of the first descendant corresponds to the original backbone towards A'' and the next step of the second descendant corresponds to the cross-link. Then, after one step, the second descendant branches into two walkers again; their trajectories correspond to the backbone of the chain $B \to B''$. The delayed branching regime is analytically tractable when we consider the FPT, as explained in Section 4.2.

Termination regime. We introduce a termination rate that controls the length of the paths. Observe that in our CGMD model, when tracing through the cross-link towards a new polymer chain, the total lengths of the two directions along $B \to B''$ sum up to $l_c = 500$. Therefore, to be fully consistent with our CGMD model, one expects that the lengths of both branches are uniformly distributed among possible choices (i.e., pairs of non-negative integers that sum up to l_c), which is technically difficult for both theoretical analysis and numerical implementation of our BRW model. Instead, we propose a (random) termination criterion that leads to similar chain lengths on average and is both analytically tractable and memory-efficient. Since each branching event corresponds to cross-linking to a new polymer chain of length l_c represented by two new paths, each path on average takes a length of $l_c/2$. Therefore, the (random) termination rate can be approximated as $\widetilde{\nu} = 2/l_c$. At each time step, each existent path terminates independently with probability $\widetilde{\nu}$, in the sense that it stops performing

random walks and no new path will be produced from it. Here, the termination event and branching event are exclusive, that is, we must have $\widetilde{\kappa} + \widetilde{\nu} \leqslant 1$. Since the length of a polymer chain of $l_c = 500$ is much larger than the possible offset distance q_x for the shortest path analysis considered here, this termination effect will be almost negligible for large branching rates.

We name the resulting integrated BRW model (with the delayed branching regime and termination) the $(\widetilde{\kappa}, \widetilde{\nu})$-BRW, where $\widetilde{\kappa}$ refers to the branching rate and $\widetilde{\nu}$ is the termination rate. Our theoretical analysis of the $(\widetilde{\kappa}, \widetilde{\nu})$-BRW model is applicable to any termination rate $\widetilde{\nu}$. We remark that with a positive termination rate, there is a nontrivial extinction probability for the spatial branching process. For this reason, in our analysis, we will always condition on the *survival event*, that there exist alive particles at all times.

Correlated jumps and mean-squared internal distance. So far, the BRW model we have discussed incorporates the jumps (i.e., link vectors between nodes) as independent and identically distributed (i.i.d.) random variables. In practice, one may expect correlations between the jumps due to the volume exclusion of the nodes in a CGMD network. To this end, we introduce the *branching correlated random walk* (BCRW) as a generalization of the BRW, where the law of a jump vector depends on the jump vector at the previous step. In the case of a branching event, for simplicity, we assume that the first step of the children depends on the jump vector of the parent walker at the previous step.[7]

To define precisely the BCRW model we need to introduce the concept of *mean-squared internal distance* (MSID). To this end, we summarize some of the key results that are well-known in polymer physics [32]. Let us consider a polymer chain of N links connecting a series of nodes whose positions are specified by the vectors $\mathbf{R}_i$, $i = 0, \ldots, N$.[8] An idealized model using classical BRW to represent the CGMD indicates that the link vectors $\mathbf{r}_i = \mathbf{R}_i - \mathbf{R}_{i-1}$ are i.i.d., resulting in $\mathbb{E}[\mathbf{r}_i \cdot \mathbf{r}_{i+1}] = 0$. Recalling that each jump length $\|\mathbf{r}_i\| = \sigma$, we have in this idealized case that $\mathbb{E}[\|\mathbf{R}_N - \mathbf{R}_0\|^2] = N\sigma^2$. However, we can introduce a measure of correlation, α, between consecutive links such that the average angle θ between consecutive links is given by $\alpha = \cos\theta$. This results in $\mathbb{E}[\mathbf{r}_i \cdot \mathbf{r}_{i+1}] = \alpha\,\sigma^2$. In general, it can be shown that $\mathbb{E}[\mathbf{r}_i \cdot \mathbf{r}_j] = \alpha^{|i-j|}\,\sigma^2$. As a result, in the case of correlated jumps, we have $\mathbb{E}[\|\mathbf{R}_N - \mathbf{R}_0\|^2] = \sum_{j=-N-1}^{N-1} \alpha^{|j|}\,\sigma^2$, which in the limit $N \to \infty$ simplifies to $\mathbb{E}[\|\mathbf{R}_N - \mathbf{R}_0\|^2] = C_\infty\, N$, where $C_\infty = (1+\alpha)/(1-\alpha)$ is called the *characteristic ratio*. The mean-squared internal distance can now be defined as

$$\mathrm{MSID}(n) = \frac{\mathbb{E}[\|\mathbf{R}_n - \mathbf{R}_0\|^2]}{n}\,. \tag{1}$$

[7] This is a simplification of the cross-linking event where the orientation of the cross-link and subsequent polymer chain (children) are not expected to be highly correlated with the original polymer chain (parent). Such an approximation affects very little the results.

[8] Typically, in this paper, a bold symbol refers to a vector.

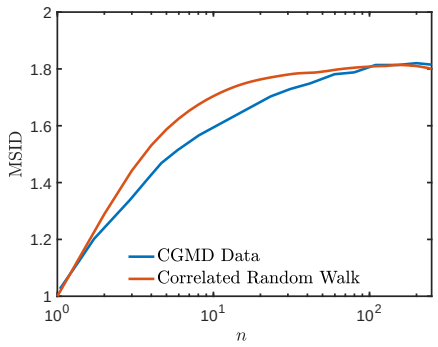

Figure 3: The MSID (in units of σ^2) computed from the CGMD model compared against the MSID of an ensemble of single chains generated using a correlated random walk.

We have $\lim_{n\to\infty} \mathrm{MSID}(n) = C_\infty$. Figure 3 (red line) shows how the MSID of a correlated random walk approaches this limit with increasing n.

We now specify the BCRW model adopted in this work. Given $\{\mathbf{r}_k\}_{1\leqslant k\leqslant i-1}$, the link vector $\mathbf{r}_i$ is specified by the following expressions

$$\mathbf{j}_i = \beta\,\mathbf{r}_{i-1} + \sqrt{1-\beta^2}\,\boldsymbol{\delta}_i,\ \ \mathbf{r}_i = \frac{\mathbf{j}_i}{\|\mathbf{j}_i\|}, \tag{2}$$

where $\beta \in (0,1)$ and $\{\boldsymbol{\delta}_i\}_{1\leqslant i\leqslant N}$ are i.i.d. samples from the unit sphere $\mathbb{S}^2$. In particular, the sequence of jump vectors $\mathbf{r}_i$ is Markovian and as a consequence, there is a computable constant $\alpha = \alpha(\beta)$ such that [33]

$$\lim_{n\to\infty} \mathrm{MSID}(n) = \frac{\sigma^2(1+\alpha)}{1-\alpha}.$$

The MSID statistics in the CGMD model (see Figure 3 blue line) can be used to determine the constant β (by inverting $\alpha(\beta)$) in the correlated random walk model. The MSID obtained from the CGMD network asymptotes to $C_\infty \approx 1.83\,\sigma^2$. We pick $\beta \approx 0.4$ in (2) so that the MSID obtained from the numerical random walk approached C_∞ in the large n limit (see Figure 3).

Another approach besides introducing correlation between jumps is to modify the jump distance σ in the BRW model so that its MSID (which is constant in n) matches that of the CGMD model at a certain value of n. A reasonable choice is $n = 1/\widetilde{\kappa}$, so that the average distance between consecutive branching points along a path in the BRW model matches the average distance between neighboring cross-linking nodes on the same chain in the CGMD model. We use the *scaled* $(\widetilde{\kappa},\widetilde{\nu})$*-BRW* to represent the BRW model whose jump distance is scaled to match the MSID at $n = 1/\widetilde{\kappa}$.

Gaussian jumps. The BCRW model with correlated jumps is not analytically convenient to deal with. However, when the effective branching rate is low, we expect from the central limit theorem (for sums of i.i.d. increments and for sums of Markov increments)

that our BRW and BCRW models both can be well approximated by a branching random walk model with independent Gaussian increments.[9] For this reason, we introduce the *Gaussian branching random walk* (GBRW) model, where by definition the jumps are i.i.d. and Gaussian distributed.[10] We incorporate the termination and delayed branching schemes, as well as proper scaling with MSID, into the GBRW model in order to stay close to the BCRW model defined above.

Our goal in introducing the GBRW model is to show that little precision is lost even if we use a simpler (and more universal) model to describe the SP statistics of a polymer network. Here, the simplicity refers to the fact that the increments are independent, and there exists a precise formula (up to $O_{\mathbb{P}}(\log\log x)$) for the FPT just as scaled BRW. The universality comes from the central limit theorem. We wish to convey the crucial idea that the correlated random walk defined in (2) should be considered as a prototype, and other similarly defined correlated random walks (e.g., using the angular fan method) that exhibit a central limit behavior (with first and second moments matching MSID calculations) should provide equally good descriptions of SP.

As a further simplification to the GBRW, we will present in Section 4.1 the theoretical treatment of the branching Brownian motion (BBM) where we prove a precise formula (up to $O_{\mathbb{P}}(1)$) for the FPT.

In the majority of our paper, we will focus on the numerical implementation of the scaled $(\widetilde{\kappa},\widetilde{\nu})$-BRW, $(\widetilde{\kappa},\widetilde{\nu})$-BCRW, and scaled $(\widetilde{\kappa},\widetilde{\nu})$-GBRW models. When there is no confusion, we simply write BRW, BCRW, and GBRW respectively. The numerical implementation of the BBM and the unscaled BRW and GBRW models are validated in Appendix B, though we do not present their performance against the CGMD results owing to their relatively poorer performance in comparison to the BRW, BCRW, and GBRW models. A summary of the four models is given in Table 1.

3. Results

The key results of the SP statistics obtained from various types of spatial branching models are discussed in this section. We start from the BCRW model which is specifically constructed to carry all three features of the CGMD network: termination, delayed branching, and correlation, following Section 2.4.[11] We then demonstrate the

[9] Meanwhile, it is well known that normal approximations sometimes behave unsatisfactorily in the large deviation regime, which applies to our case since we will be interested in the extremal behavior of the spatial branching models. It is therefore risky to apply the aforementioned heuristic of the central limit theorem. Fortunately, when the branching rate is sufficiently small (which is the case for the polymeric systems in which we are interested) and the offset distance q_x is not too large, we are in a relatively moderate deviation regime, and the normal approximation shows quite good precision.

[10] The increments of a GBRW model are independent, meaning that it fails to capture the correlation between the jumps on distinct cross-linked chains when compared to the BCRW model. Nevertheless, this does not hamper the FPT statistics significantly; see Figure 12(a) below.

[11] We slightly abuse notation here by including the delayed branching property in BRW, where we also assume that jumps are uniform on $\mathbb{S}^2$; instead, the traditional BRW (i.i.d. offsprings) will be referred to the *classical* BRW.

Model	BCRW	BRW	GBRW	BBM
Time variable	discrete	discrete	discrete	continuous
Jumps	dependent	independent	independent	independent
Jump distribution	uniform on $\mathbb{S}^2$	uniform on $\mathbb{S}^2$	Gaussian	Gaussian
Jumps $\propto \sqrt{\text{MSID}}$	N/A	✓	✓	✓
Termination	✓	✓	✓	N/A
Delayed branching	✓	✓	✓	N/A
FPT predictions	not available	$\pm O(\log\log x)$	$\pm O(\log\log x)$	$\pm O(1)$

Table 1: A summary of the characteristics of the four spatial branching models considered in this work

scaled BRW and GBRW models,[12] which are more tractable and have an equally good description of the SP statistics. In particular, for the BRW and GBRW models, we will be able to develop asymptotic formulas for the FPT, which leads to useful theoretical predictions in Section 4.2.

3.1. SP statistics predicted by BCRW

Numerical results. Using the method described in Section 2.3, the effective branching rate corresponding to the CGMD model containing 250,000 beads with 6,000 cross-links is $\widetilde{\kappa} \approx 0.0398$ and that with 13,600 cross-links is $\widetilde{\kappa} \approx 0.0856$. Figure 4 shows the SP distribution (for $q_x \approx 65.5\,\sigma$) from the CGMD model and that predicted by the BCRW model at these two cross-linking densities. Good agreement is observed between the CGMD results and BCRW predictions, both in terms of the mean and the standard deviation.

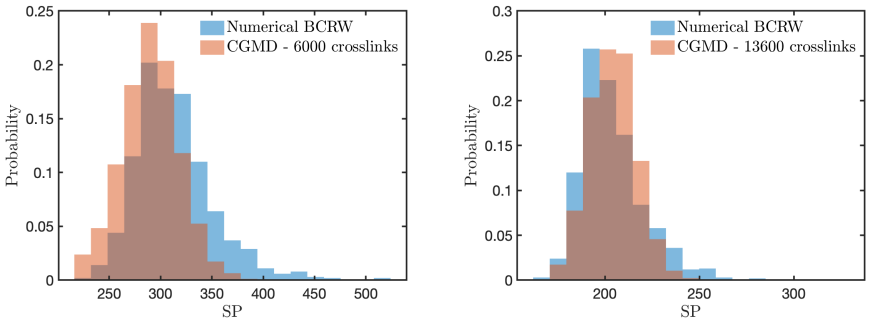

(a) (b)

Figure 4: The SP distributions from the BCRW compared against a single CGMD configuration at different cross-link densities: (a) 6000 cross-links ($\widetilde{\kappa} \approx 0.0398$), and (b) 13600 cross-links ($\widetilde{\kappa} \approx 0.0856$) for $q_x = 65.5\,\sigma$ (≈ 98.2 nm).

Figure 5(a) shows how the SP distribution predicted by the BCRW model depends

[12] By *scaled* we mean that the jumps (positions of subsequent particles in the tree) are scaled by a common factor.

on the offset distance q_x. The distribution shifts to the right with its shape nearly unchanged with increasing q_x, in good agreement with the CGMD result shown in Figure 1(b). Figure 5(b) shows that the mean SP grows linearly with q_x, with excellent agreement between BCRW and CGMD models. Figure 5(c) shows that the standard deviation of SP remains almost unchanged in the range of q_x considered here, with the BCRW prediction a little higher than the CGMD results. In summary, the BCRW model successfully captures the linear dependence of the SP mean with q_x and the CGMD observation that the SP standard deviation stays near a constant value much smaller than the mean.[13] We note that the correlation between successive jumps is important for reaching the level of agreement between BCRW and CGMD predictions shown here. If the correlation were simply removed (not shown), then the SP mean would become larger (the FPT increases since uncorrelated jumps make the trajectory more tortuous), while the standard deviation would remain largely unchanged and independent of q_x.

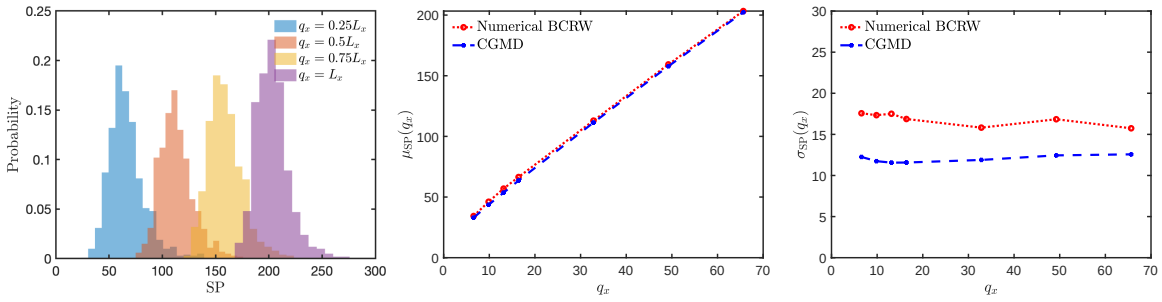

(a) (b) (c)

Figure 5: (a) The SP distributions at different values of q_x from the numerical BCRW. The (b) mean and (c) standard deviation of the SP as a function of q_x. The data points correspond to $q_x = 0.1L_x$, $0.15L_x$, $0.2L_x$, $0.25L_x$, $0.5L_x$, $0.75L_x$, L_x. All network analysis corresponds to a single CGMD configuration with a cross-link density that corresponds to $\widetilde{\kappa} = 0.0856$ in the BCRW model.

Metric for linear dependence of SP on q_x. Figure 5(b) suggests that in the range of q_x considered here, the SP mean can be well approximated by a linear relation,

$$\mu_{\rm SP}(q_x) = \frac{q_x}{\overline{c}_1} + b \tag{3}$$

where $\overline{c}_1$ is the inverse of the slope and b is the intercept. We expect this relation to be well obeyed as long as q_x is not too small. The $\overline{c}_1$ and b parameters can be extracted from the $\mu_{\rm SP}(q_x)$ data, as shown in Figure 5(b) by linear regression.[14] We note that

[13] That the FPT of BCRW is concentrated can be supported intuitively by the following famous quote from [34]: *A random variable that depends (in a "smooth" way) on the influence of many independent variables (but not too much on any of them) is essentially constant.*

[14] For the linear regression fit, we compute the $\mu_{\rm SP}$ for $q_x = 0.25L_x$, $0.5L_x$, $0.75L_x$, L_x. We will later see in (13) that an extra logarithm correction term is expected. However, since the logarithmic

the intercept b is relatively small (compared against $q_x/\overline{c}_1$) and is on the order of σ_{SP}. Hence the parameter $\overline{c}_1$ allows us to have a quick estimate of the SP mean, which is fairly accurate at large q_x.

The parameter $\overline{c}_1$ is a key property; larger $\overline{c}_1$ means straighter shortest path. Within the BRW models, $\overline{c}_1$ can be interpreted as the 'speed' of the shortest paths; a larger $\overline{c}_1$ corresponds to greater distances that the shortest paths can reach per unit time. If we ignore b, which is small, then $\overline{c}_1$ is a measure of the straightness of the shortest paths, and the inverse of $\overline{c}_1$ is the *tortuosity*. As we shall discuss in Section 4.3, the inverse of $\overline{c}_1$ corresponds to an important physical parameter that measures the maximum stretch that can be applied to the polymer network before significant bond-breaking events must occur.

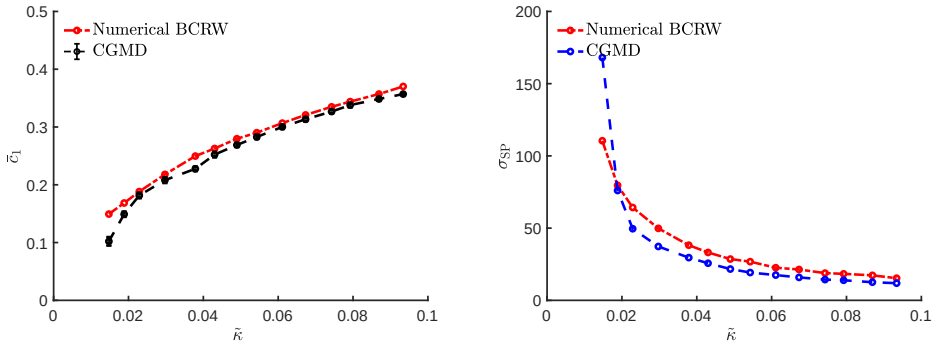

(a) (b)

Figure 6: (a) $\overline{c}_1$ averaged over 10 independent CGMD configurations compared against the BCRW at different cross-link densities (corresponding to branching rate $\widetilde{\kappa} \in [0.0148, 0.0934]$). (b) Comparison of the standard deviations of the SP distribution from the CGMD simulation and of the FPT distribution from the numerical BCRW.

Figure 6(a) plots $\overline{c}_1$ as a function of the branching rate $\widetilde{\kappa}$ from both the BCRW and the CGMD models. (The cross-link density of typical elastomers corresponds to $\widetilde{\kappa}$ values lower than the maximum value considered here.) The CGMD results are obtained by averaging over 10 configurations at each cross-link density. The $\overline{c}_1$ prediction of the BCRW model agrees well with the CGMD model, especially at a high branching rate $\widetilde{\kappa}$. In general, $\overline{c}_1$ increases with $\widetilde{\kappa}$, indicating that the shortest paths become straighter at a higher cross-link density. The overall shape of the $\overline{c}_1$-$\widetilde{\kappa}$ relation resembles that of a square root function. This is not a coincidence; in Section 4 we will show that if certain simplifications are introduced, the relationship becomes exactly a square root. Figure 6(b) plots the standard deviation σ_{SP} of the shortest paths as a function of $\widetilde{\kappa}$ from both the BCRW and the CGMD models for $q_x = L_x$. Here, the prediction from the BCRW model also shows qualitative agreement with the CGMD model. In general, σ_{SP} decreases with $\widetilde{\kappa}$, indicating that the shortest path distribution becomes

function grows very slowly, this extra term can be well described by the linear and constant terms in the linear regression estimate for the range of q_x we use in our presented analysis.

more concentrated at a higher cross-link density. The intercept b also decreases with increasing $\widetilde{\kappa}$, as shown in Appendix C.

3.2. SP statistics predicted by scaled BRW

While the BCRW model in Section 3.1 can successfully capture the SP statistics in the polymer network, the correlation between jumps is difficult to account for in the theoretical analysis. To circumvent these difficulties, we introduced simplified models such as scaled BRW, where individual increments are independent but the jump distance is scaled to match the MSID at $n = 1/\widetilde{\kappa}$ (scaling the jump as $\sigma_s = \sqrt{\mathrm{MSID}(1/\widetilde{\kappa})}\,\sigma$). This simplification makes theoretical predictions on SP possible (see Section 4.2).

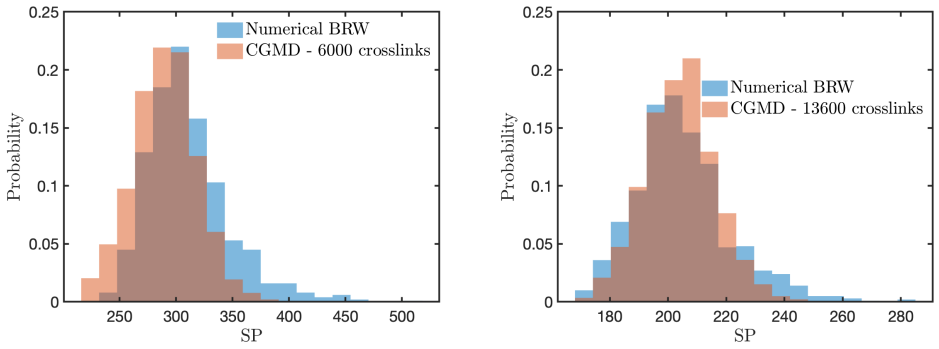

(a) (b)

Figure 7: The SP distributions compared against a single CGMD configuration from the scaled BRW at different cross-link densities: (a) 6000 cross-links ($\widetilde{\kappa} \approx 0.0398$), and (b) 13600 cross-links ($\widetilde{\kappa} \approx 0.0856$) for $q_x = 65.5\,\sigma$ (≈ 98.2 nm).

Numerical results. Figure 7 shows the FPT distribution predicted by the scaled $(\widetilde{\kappa}, \widetilde{\nu})$-BRW model, which is in good agreement with the SP distribution from the CGMD configuration with 6000 cross-links ($\widetilde{\kappa} = 0.0398$) and 13600 cross-links ($\widetilde{\kappa} = 0.0856$). The scaled BRW performs much better than the unscaled BRW (not shown in this paper) and does comparably as well as the BCRW from Section 3.1. This is because by scaling jump steps to match the MSID at a $n = 1/\widetilde{\kappa}$, the expansion of the BRW tree in space is just as fast as the BCRW tree, thereby capturing a similar FPT or SP behavior.

Figure 8(a) shows that the scaled BRW successfully captures the change in the SP distribution for different offset distances q_x (at branching rate $\widetilde{\kappa} = 0.0856$). Figure 8(b) shows that its prediction of mean SP as a function of q_x agrees very well with the CGMD result. Figure 8(c) shows that the predicted width of the SP distribution stays nearly constant in agreement with CGMD. From the linear dependence of mean SP on q_x, we compute the $\overline{c}_1$ at different $\widetilde{\kappa}$ from the scaled BRW model, as shown in Figure 9(a). Figure 9(b) shows the σ_{SP} at $q_x = L_x$ as a function of different $\widetilde{\kappa}$. These results are in good agreement with the CGMD results and demonstrate that the independence of the jumps in the BRW model does not affect the statistics as long as the jumps are scaled to reproduce the MSID at $n = 1/\widetilde{\kappa}$.

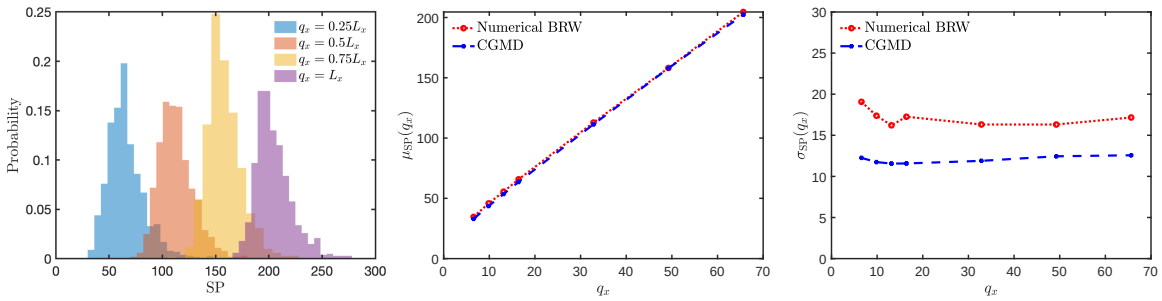

(a) (b) (c)

Figure 8: (a) The SP distributions at different values of q_x from the numerical BRW. The (b) mean and (c) standard deviation of the SP as a function of q_x. The data points correspond to $q_x = 0.1L_x$, $0.15L_x$, $0.2L_x$, $0.25L_x$, $0.5L_x$, $0.75L_x$, L_x. All network analysis corresponds to a single CGMD configuration with a cross-link density corresponding to $\widetilde{\kappa} = 0.0856$ in the BRW model.

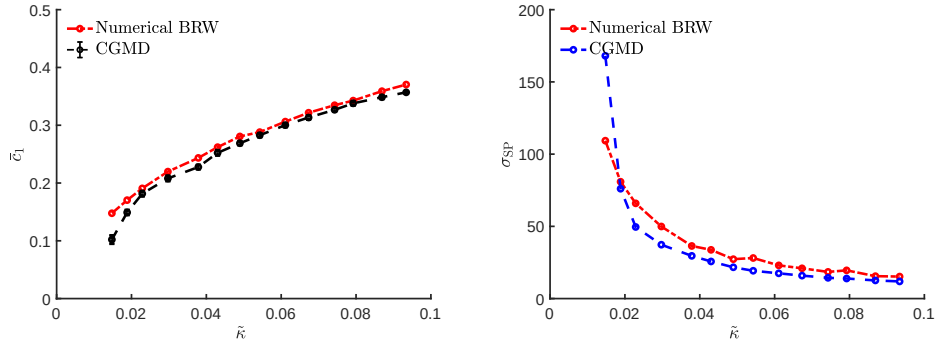

(a) (b)

Figure 9: (a) $\overline{c}_1$ averaged over 10 independent CGMD configurations compared against the scaled BRW at different branching rates $\widetilde{\kappa}$. (b) Comparison of the standard deviations of the SP distribution from the CGMD simulation and of the FPT distribution from the numerical BRW.

3.3. SP statistics predicted by GBRW

In this section, we present the numerical results of the GBRW model, which makes the further approximation that the random walk steps satisfy Gaussian distribution, in addition to being independent. In order to match the MSID of the CGMD model at $n = 1/\widetilde{\kappa}$, the incremental distribution of the GBRW model is given by the 3-dimensional centered Gaussian distribution with covariance matrix $\sqrt{\mathrm{MSID}(1/\widetilde{\kappa})/3}\, I_3$, where I_3 is the 3×3 identity matrix.

Numerical results. Figure 10 shows the FPT distribution predicted by the scaled $(\widetilde{\kappa}, \widetilde{\nu})$-GBRW model, which is in good agreement with the SP distribution from the CGMD configuration with 6000 cross-links ($\widetilde{\kappa} = 0.0398$) and 13600 cross-links ($\widetilde{\kappa} = 0.0856$).

Figure 11(a) shows that the scaled GBRW successfully captures the change in the SP distribution for different offset distance q_x (at branching rate $\widetilde{\kappa} = 0.0856$). Figure 11(b) shows that its prediction of mean SP as a function of q_x agrees very well with the CGMD

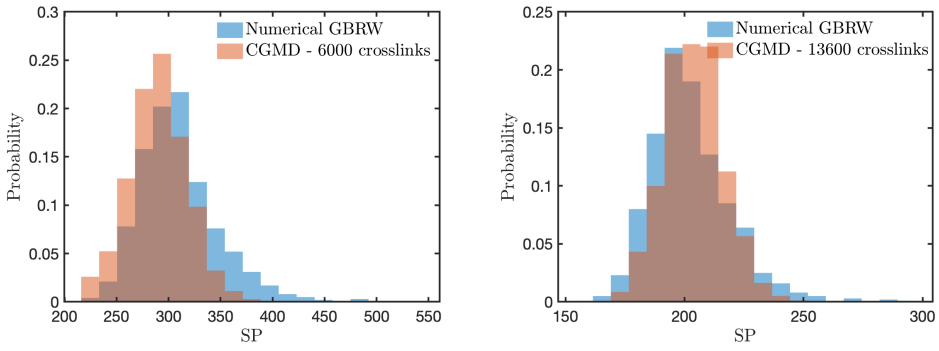

(a) (b)

Figure 10: The SP distributions compared against a single CGMD configuration from the numerical GBRW at different cross-link densities: (a) 6000 cross-links ($\widetilde{\kappa} \approx 0.0398$), and (b) 13600 cross-links ($\widetilde{\kappa} \approx 0.0856$) for $q_x = 65.5\,\sigma$ (≈ 98.2 nm).

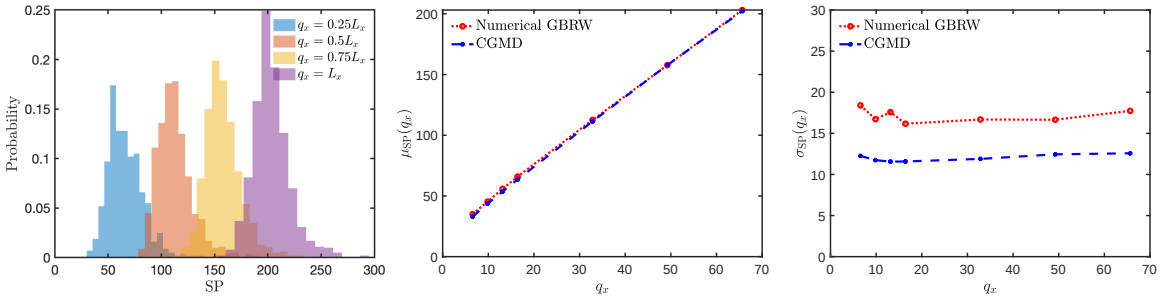

(a) (b) (c)

Figure 11: (a) The SP distributions at different values of q_x from the numerical GBRW. The (b) mean and (c) standard deviation of the SP as a function of q_x. The data points correspond to $q_x = 0.1L_x$, $0.15L_x$, $0.2L_x$, $0.25L_x$, $0.5L_x$, $0.75L_x$, L_x. All network analysis corresponds to a single CGMD configuration with a cross-link density corresponding to $\widetilde{\kappa} = 0.0856$ in the GBRW model.

result. Figure 11(c) shows that the predicted width of the SP distribution stays nearly constant in agreement with CGMD. From the linear dependence of mean SP on q_x, we compute the $\overline{c}_1$ at different $\widetilde{\kappa}$ from the scaled GBRW model, as shown in Figure 12(a). Figure 12(b) shows the $\sigma_{\rm SP}$ at $q_x = L_x$ as a function of different $\widetilde{\kappa}$. These results are in good agreement with the CGMD results and demonstrate that the independence and Gaussian distribution of the jumps in the GBRW model do not affect the statistics as long as the jumps are scaled to reproduce the value of MSID at $n = 1/\widetilde{\kappa}$.

4. Analytical predictions and conjectures on first passage times

The numerical analysis of the BRW models in Section 3 demonstrated that they can capture the essential statistics of shortest paths in a polymer network. Here we will show that some of these models (BRW and GBRW) are analytically treatable, i.e. we can obtain analytic expressions on their first passage time (FPT) statistics. These

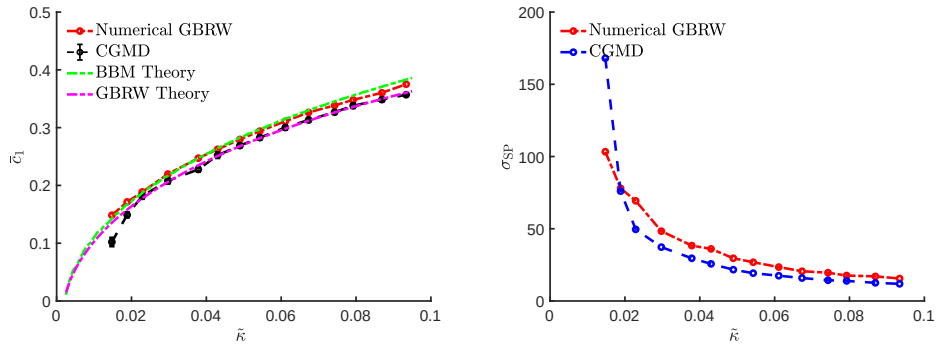

(a) (b)

Figure 12: (a) $\overline{c}_1$ averaged over 10 independent CGMD configurations compared against the numerical GBRW at different branching rates $\widetilde{\kappa}$. The curves labeled *Theory* refer to the analytic predictions of the FPT established in Section 4. Here, the *BBM Theory* curve represents a proxy for the GBRW using BBM with a modified branching rate based on the termination and delayed branching regimes. Appendix E. (b) Comparison of the standard deviations of the SP distribution from the CGMD simulation and of the FPT distribution from the numerical GBRW.

analytic results would provide not only a deeper understanding of the statistical behavior of shortest paths in polymer networks but also a convenient way to estimate the SP lengths given the cross-link density. Our analysis establishes a connection between polymer physics and the extensive literature on the extremal behavior of spatial branching processes. In particular, the inverse of parameter $\overline{c}_1$ determines the critical stretch that can be applied to the polymer before extensive bond-breaking events occur. Our analysis shows that classical polymer models that assume a periodic network topology (such as the 8-chain model) predict a much longer mean SP for a given offset distance q_x, hence a much larger critical stretch, compared to the more realistic models of polymer networks where cross-links are introduced randomly.

4.1. First passage times of branching Brownian motion

Starting from the GBRW model considered in Section 3.3, if we introduce a further modification where the time becomes a continuous variable (instead of being integers), then we arrive at the branching Brownian motion (BBM) model, which is even more convenient for theoretical analysis. In the BBM model, the trajectory of each particle follows the Wiener process in $\mathbb{R}^d$ and they can produce new particles at any time with a fixed branching rate. Here we define the standard BBM where the branching is binary (each branching event turns one particle into two) and the branching rate is $\widetilde{\kappa} = 1$ (and zero termination rate, $\widetilde{\nu} = 0$). Denote by M_t the maximal displacement of the one-dimensional standard BBM at time t. A classical result of [16] shows that

$$M_t = \sqrt{2}\,t - \frac{3}{2\sqrt{2}}\log t + O_{\mathbb{P}}(1). \tag{4}$$

In the following, we present our theoretical results on FPT asymptotics for BBM and compare them against (4). We denote by B_x the d-dimensional ball of radius one

centered at $(x, 0, \ldots, 0) \in \mathbb{R}^d$, which is our termination criterion for the BBM.

Theorem 1 (FPT for standard BBM)**.** *The first passage time τ_x for the standard BBM in dimension $d \geqslant 1$ to B_x is given by*

$$\tau_x = \frac{x}{\sqrt{2}} + \frac{d+2}{4} \log x + O_{\mathbb{P}}(1), \tag{5}$$

where by definition, the $O_{\mathbb{P}}(1)$ term is tight.[15]

The proof of this theorem is given in Appendix A.1. To achieve greater mathematical generality, we may use a standard scaling argument to obtain the following asymptotes for BBM with a generic branching rate κ (different from the branching rate $\widetilde{\kappa}$ for the BRW) and a generic diffusivity constant s (different from the step size σ for the BRW).[16]

Corollary 2 (FPT for BBM)**.** *Consider a BBM in $\mathbb{R}^d$ with branching rate $\kappa > 0$ and diffusivity $s > 0$, then its first passage time $\tau_{\kappa,s}(x)$ to B_x is given by*

$$\tau_{\kappa,s}(x) = \frac{x}{s\sqrt{2\,\kappa}} + \frac{d+2}{4\,\kappa} \log\left(\frac{x}{s}\right) + O_{\mathbb{P}}(1), \tag{6}$$

where by definition, the $O_{\mathbb{P}}(1)$ is tight in x for each fixed κ and s.

Corollary 2 has a number of consequences that lead to a better understanding of the BRW models. As a simple example, we showcase how the delayed branching BRW with uniform jumps on $\mathbb{S}^2$ can be approximated using a BBM. The quantity x in (6) corresponds to the q_x in the SP and FPT analysis in the previous sections, and the first two terms on the right-hand side of (6) correspond to $\mu_{\mathrm{SP}}(q_x)$. Since BBM is isotropic in 3 dimensions, the central limit theorem yields that each step of the BRW can be approximated by a Gaussian vector $\mathrm{N}(\mathbf{0}, \sigma^2 I_3/3)$. In other words, we apply Corollary 2 with diffusivity $s = \sigma/\sqrt{3}$. Next, we will derive in Appendix E that the BBM branching rate κ well approximates a BRW branching rate $\widetilde{\kappa}$ if κ solves $e^{\kappa}(\kappa + \widetilde{\nu}) = 2\,\widetilde{\kappa}$. Note that in the limit of $\widetilde{\nu}, \widetilde{\kappa} \to 0$, we have the approximation $\kappa \approx 2\,\widetilde{\kappa}$ (this is because, in our BRW models, every branching event produces two new particles instead of one new particle in the standard BBM model).

The asymptotic (6) will be numerically validated in Appendix B.2 for diffusivity $s = 1$, which corresponds to a random walk with jump length of $\sqrt{3}$. We leave it as a mathematical challenge for future studies to analyze the structure of the $O_{\mathbb{P}}(1)$ term: whether it converges in law, and even whether it is of the form $c + o_{\mathbb{P}}(1)$ for some constant c (as is the case for the one-dimensional maximum M_t). We note that (6) provides a

[15] A family of random variables $\{Z_x\}_{x \geqslant 0}$ is *tight* if for every $\varepsilon > 0$ there are constants $b, x_0 > 0$ such that $\sup_{x > x_0} \mathbb{P}(|Z_x| > b) < \varepsilon$.

[16] By definition, a Brownian motion of diffusivity s is equivalent in distribution to a standard Brownian motion scaled by s. In other words, the variance at time t is $s^2 t$.

theoretical justification for our numerical finding that the standard deviation of SP in the polymer network is much less than its mean at large q_x.

The right-hand side of (6) for the FPT $\tau_{\kappa,s}(x)$ does not appear to be linear in x, in contrast to (3). In the limit as $x \to \infty$, the quantity $\overline{c}_1$ approximately equals $s\sqrt{2\,\kappa}$ where $s = \sqrt{\mathrm{MSID}(1/\widetilde{\kappa})/3}$, whereas in the linear fitting executed in our numerical analysis, the effect from the logarithm term is not negligible at $x = q_x$. Nonetheless, we can still use (6) to provide an estimate of the $\overline{c}_1$ parameter obtained from the linear fit,

$$\overline{c}_1 \approx \left(\frac{1}{s\,\sqrt{2\,\kappa}} + \frac{d+2}{4\kappa\,\hat{q}_x} \right)^{-1} . \tag{7}$$

where $\hat{q}_x$ lies somewhere inside the range of q_x where the linear fit is performed.

4.2. Conjectural asymptotics for branching random walk models

In Section 4.1, we established the asymptotes for the maximum (4) and the FPT (5) for the BBM. In particular, the asymptote (5) with $d = 1$ is precisely the inversion of (4), in the sense that $M_{\tau_x} \approx x$ and $\tau_{M_t} \approx t$. This crucial *inversion relation* motivates several conjectures for the FPT of the BRW models of interest. Before stating these conjectures, we need to understand the asymptotics of the maximum of the BRW models we introduced.

The key difference between BRW and BBM models is that in BRW the time is discrete, which makes the analysis more difficult. We will use integer n to represent the time in BRW models. In the following, we will state a theorem on the maximal displacement for the BRW models, which should be compared against (4). We will work in a general dimension $d \geqslant 1$ and only impose mild assumptions on the jump distribution, while the termination and delayed branching schemes remain. First, we introduce a large deviation rate function to characterize the jump vector $\boldsymbol{\xi}$ at each step of the BRW models. We assume that the distribution of $\boldsymbol{\xi}$ is rotationally invariant. Denote by ξ the first coordinate of $\boldsymbol{\xi}$, which is a real-valued random variable. The large deviation rate function is defined as

$$I(x) := \sup_{\lambda > 0} \Big(\lambda x - \log \phi_\xi(\lambda) \Big), \tag{8}$$

where $\phi_\xi(\lambda) := \mathbb{E}[e^{\lambda \xi}]$ is the moment generating function for ξ (we assume implicitly that this is well-defined for $\lambda \in \mathbb{R}$). For example, for the (unscaled) GBRW model we have $I(x) = x^2/2$.

Theorem 3 (maxima for one-dimensional delayed branching BRW)**.** *In the above setting, suppose that $(\widetilde{\kappa}, \widetilde{\nu})$ satisfies $\widetilde{\kappa} + \widetilde{\nu} \leqslant 1$ and $2\widetilde{\kappa}(1 - \widetilde{\nu}) > \widetilde{\nu}$. Let M_n denote the maximum of the first coordinate of the $(\widetilde{\kappa}, \widetilde{\nu})$-BRW. Conditioned upon survival,*

$$M_n = c_1 n - \frac{3}{2\,c_2} \log n + O_{\mathbb{P}}(1)\,, \tag{9}$$

where

$$\rho := \rho(\widetilde{\kappa}, \widetilde{\nu}) = \frac{1-\widetilde{\nu}}{2} + \sqrt{\frac{(1-\widetilde{\nu})^2}{4} + 2\widetilde{\kappa}(1-\widetilde{\nu})} \tag{10}$$

and c_1 *and* c_2 *are constants satisfying the following equations:*

$$\begin{aligned} I(c_1) &= \log \rho \,, \\ c_2 &= I'(c_1) \,. \end{aligned} \tag{11}$$

For example, for the (unscaled) GBRW model we have $c_1 = c_2 = \sqrt{2 \log \rho}$. The form of (10) is slightly more involved due to the delayed branching property. Indeed, for BRW without delayed branching, (10) is replaced by $\rho = 1 + 2\widetilde{\kappa} - \widetilde{\nu}$, a well-known result in the literature [12]. A derivation of the formula (10) can be found in the proof of Lemma 5 in Appendix A.2.

Intuitively, ρ is the parameter that indicates the rate of growth of the number of particles: at time n, we expect that the number of particles grows like ρ^n conditioned upon survival. The existence and uniqueness of c_1 in (11) is a consequence of the assumption $2\widetilde{\kappa}(1-\widetilde{\nu}) > \widetilde{\nu}$. Indeed, this implies $\rho > 1$, and we recall that I is strictly increasing, concave, and continuous on $[0, \infty)$, and $I(0) = 0$.

For a large n, the linear coefficient c_1 in (9) describes the effective velocity of the maximum of the BRW. Let us briefly explain why intuitively we expect that the effective velocity c_1 satisfies $I(c_1) = \log \rho$. Suppose that the locations of the particles at time n are independent.[17] By Cramér's theorem (see [35]), the probability of finding a certain particle located around $c_1 n$ at time n is roughly $e^{-(I(c_1)+o(1))n}$. Since we expect around ρ^n particles at time n, the total number of particles near $c_1 n$ at time n can be estimated by $\approx \rho^n e^{-I(c_1)n} = 1$, meaning that the maximum reach of the particles is close to $c_1 n$ at time n.

It is instructive to compare (9) with (4). For example, (9) reduces to (4) if $c_1 = c_2 = \sqrt{2}$. Intuitively, we may consider BBM as a generalization of the GBRW model (i.e. with Gaussian increments) with $I(x) = x^2/2$ to continuous time. For a standard BBM model, we expect the number of particles to grow as e^t, and hence $\rho = e$. This amounts to $c_1 = c_2 = \sqrt{2 \log \rho} = \sqrt{2}$.

In view of the inversion relation in the BBM model between the FPT in (5) and the maximal displacement in (4), we pose the following conjecture for the BRW model.

Conjecture 1 (FPT for delayed branching BRW)**.** In the above setting, suppose that $(\widetilde{\kappa}, \widetilde{\nu})$ satisfies $\widetilde{\kappa} + \widetilde{\nu} \leqslant 1$ and $\rho(\widetilde{\kappa}, \widetilde{\nu}) > 1$. Conditioned upon survival, the first passage time τ_x to B_x satisfies the asymptotic

$$\tau_x = \frac{x}{c_1} + \frac{d+2}{2c_2 c_1} \log x + O_{\mathbb{P}}(1). \tag{12}$$

[17] Of course, this is a wrong hypothesis, since two paths have the same displacements before they branch. This partly explains the logarithm correction term.

In a companion paper [36], we prove a slightly weaker version of (12), with the $O_{\mathbb{P}}(1)$ term replaced by $O_{\mathbb{P}}(\log\log x)$ under certain mild assumptions on $\boldsymbol{\xi}$ (that applies for uniform distribution on $\mathbb{S}^2$ and Gaussian distribution on $\mathbb{R}^3$). That is, we prove that conditioned upon survival,

$$\tau_x = \frac{x}{c_1} + \frac{d+2}{2c_2c_1}\log x + O_{\mathbb{P}}(\log\log x). \tag{13}$$

The asymptotic relation (13) is confirmed numerically in Appendix B.1.

The formula (13) provides the analytic prediction of the quantity $\overline{c}_1$ that can be compared against the CGMD results, as shown in Figure 12(a). As remarked above, c_1 becomes $\overline{c}_1$ only in the limit of $x = q_x \to \infty$. At a finite offset distance q_x, the logarithm term in (13) is not negligible,

$$\overline{c}_1 \approx \left(\frac{1}{c_1} + \frac{d+2}{2c_1c_2\,\hat{q}_x}\right)^{-1}, \tag{14}$$

where $\hat{q}_x$ lies somewhere inside the range of q_x where the linear fit is performed. Figure 12(a) shows the analytic prediction of $\overline{c}_1$ (for $\hat{q}_x = L_x/2$) as a function of $\widetilde{\kappa}$ for the BBM model (see (7)) and the GBRW model (see (14)), which is in good agreement with both the numerical implementation of GBRW model and the CGMD results.

4.3. Critical stretch and comparison with classical periodic network model for polymers

The theoretical analysis for the BBM, GBRW, and BRW models above provides an accurate estimate of the FPT distribution that explains the SP distribution in a polymer network given the cross-link density from the CGMD simulations. The mean SP, in particular the parameter $\overline{c}_1$, determines the stretchability of the elastomer before the onset of significant bond-breaking events. To see why this is the case, consider a shortest path of contour length L_{SP} connecting two nodes at distance q_x apart. If a stretch λ is applied to the network but no bonds break, then the two nodes are separated by $\lambda\, q_x$ and the shortest path contour length stays at L_{SP}. Because the end-to-end distance of a shortest path can never be stretched longer than its contour length, we have $\lambda\, q_x \leqslant L_{\mathrm{SP}}$, i.e. $\lambda \leqslant L_{\mathrm{SP}}/q_x \approx 1/c_1$. Therefore, we can define $\lambda_c = 1/c_1$ as the critical stretch that can be applied to the elastomer before extensive bond-breaking occurs.

We now discuss how the critical stretch λ_c depends on the cross-link density, characterized by parameter $\widetilde{\kappa}$. For simplicity, here we shall ignore the effect of correlation between consecutive jumps in the random walk, i.e., modeling the polymer chain as an uncorrelated random walk ($\sigma = 1$). We pick the BBM model (at $d = 3$) with unit jump length (corresponding to $s = \sqrt{1/3}$), where the analytic expression is the simplest. In the limit of $\widetilde{\nu}, \widetilde{\kappa} \to 0$, $\kappa \approx 2\widetilde{\kappa}$. In the limit of large q_x, we have $c_1 \to s\sqrt{2\kappa} \approx \sqrt{4\,\widetilde{\kappa}/3}$ and hence

$$\lambda_c^{\mathrm{BBM}} \approx \sqrt{\frac{3}{4\,\widetilde{\kappa}}}\,. \tag{15}$$

On the other hand, if one assumes the periodic network structure of the 8-chain (a.k.a. Arruda-Boyce) model [6], it can be easily shown that $c_1 = \sqrt{\widetilde{\kappa}/3}$ and hence[18]

$$\lambda_c^{\text{8-chain}} \approx \sqrt{\frac{3}{\widetilde{\kappa}}}. \tag{16}$$

Note that both models predict the same $\widetilde{\kappa}^{-1/2}$ scaling with the cross-link density. However, $\lambda_c^{\text{8-chain}}/\lambda_c^{\text{BBM}} \approx 2$. This means that relative to the more realistic model that accounts for the random distribution of cross-links, the 8-chain model overestimates the critical stretch for extensive bond-breaking by about a factor of 2 (in the limit of $q_x \to \infty$, $\widetilde{\nu}, \widetilde{\kappa} \to 0$, see Appendix D for comparison against other spatial branching models).

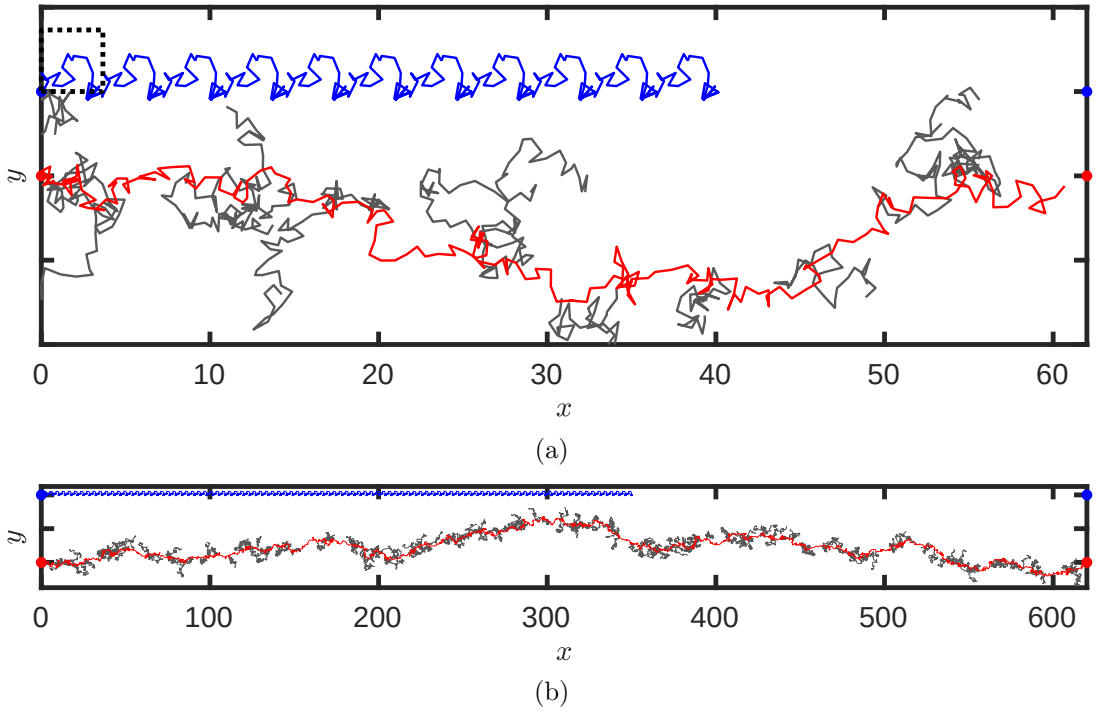

Figure 13: Shortest path trajectory for the BRW model (red path with selected branches shown in black) and 8-chain model (blue path) at $\widetilde{\kappa} = 0.1$ for the same amount of time it takes for the BCRW path to reach its destination for (a) $q_x = 62$ and (b) $q_x = 620$.

To provide an intuitive understanding of the difference between BRW (approximated by the BBM estimates in (6)) and the periodic model of the polymer network, we look at the trajectory of the shortest path from the BRW model and the 8-chain model

[18]Strictly speaking, within the 8-chain model, the contour length of the shortest path can never be exactly straight because it must pass through the body-center of the unit cell. Accounting for this constraint leads to an implicit equation for the critical stretch, $\lambda_c^2 + 2/\lambda_c = 3/\widetilde{\kappa}$, the solution of which is close to (16) in the limit of large λ_c.

for $\widetilde{\kappa} = 0.1$ and $\widetilde{\nu} = 2/500$ for which $\kappa \approx 1.65\,\widetilde{\kappa}$. Here we expect from (6) that $\lambda_c^{\text{8-chain}}/\lambda_c^{\text{BBM}} \approx 1.82$ (in the limit of $q_x \to \infty$). Figure 13(a) shows the trajectory of the shortest path generated by the BRW model (shown in red). A few side branches connected to the shortest path are shown in black. In this case, the mean shortest path is able to reach a distance of $q_x = 62$ in 220 steps. The blue path in Figure 13(a) shows the shortest path in a network consisting of periodic repeating cells (dashed line) each containing eight chains (only two chains are shown for clarity). In this case, the shortest path only reaches a distance of $q_x^{\text{8-chain}} \approx 40$ in 220 steps. In other words, the shortest path in the 8-chain model of the polymer network is much more tortuous than that predicted by the more realistic BRW models. As a result, the 8-chain model would overestimate the critical stretch by which extensive bond-breaking events occur. Here, the ratio of the distance covered in the same duration as the FPT of the BRW ($q_x/q_x^{\text{8-chain}}$) is $\approx 62/40 \approx 1.54$. On increasing the q_x to 620, this ratio increases to ≈ 1.77, as shown by the paths in Figure 13(b). This is smaller than the theoretical estimate of $\lambda_c^{\text{8-chain}}/\lambda_c^{\text{BBM}} \approx 1.82$ because in this illustration q_x is still relatively small. We have numerically verified that for a very large offset distance q_x the limit $\lambda_c^{\text{8-chain}}/\lambda_c^{\text{BBM}} \approx 1.82$ is indeed recovered.

The 8-chain model has been very successful in predicting the elastic (i.e. reversible) responses of elastomers, which is the result of the aggregated response of all polymer chains in the network. However, at the critical stretch, λ_c, we are entering the regime of irreversible strain-induced damage. In this regime, the polymer chains that lie on the shortest paths play a decisive role because they constrain the maximum stretch that can be applied unless bond breaking occurs. The spatially branching processes provide a more realistic description of the length distribution of shortest paths and hence a more physical description of the polymer as it enters the irreversible strain-induced damage regime.

5. Conclusions and outlook

In this paper, we present a class of branching random walk (BRW) models whose first passage time (FPT) statistics are used to generate shortest path length (SP) statistics to understand the structure of polymeric networks as modeled by CGMD simulations. The effective branching rate (for a given cross-link density) in our BRW models is obtained from the inter-cross-link chain length distribution from the CGMD simulation cell. We analyze the FPT of the BRW and relevant models from both numerical and theoretical aspects. The numerical simulations show that multiple BRW models, with various levels of idealizations, are able to reproduce the SP distribution (in terms of both mean and standard deviation) of the polymer model as modeled by CGMD. Our theory yields an explicit relation between the mean SP (FPT) and the offset distance q_x as a function of the cross-link density. The theoretical estimate validates the results from our numerical approach and is in good agreement with the CGMD calculations. The FPT or SP dependency on the offset distance at equilibrium serves as an indicator of the stretch limit or stretchability of the polymer. The theoretical estimate of the FPT from the spatial branching processes shows a much lower stretch limit as compared to

idealized representations of polymer networks using periodic repeating structures. This shows that treating the polymer network as a BRW captures a more realistic response of the material response in the regime of extensive bond-breaking.

In this paper, we have analyzed polymer networks prepared at equilibrium, before any deformation and strain-induced damage, and the SP distribution is expected to be isotropic. As a result, the BRW has been modeled with isotropic jumps in space. The next step is to see whether the BRW models can be used to understand the evolution of SP statistics as bonds break by deformation. In elastomers with irreversible cross-links, we hypothesize that the reduction in the number of bonds (cross-link density) with loading may be modeled by a modification in the branching rate of the BRW or by introducing anisotropy in the jumps as governed by the directional dependence of the SP. Reversibly cross-linked systems present a challenge since there is no reduction in the cross-link density (broken cross-links readily reform at ultrafast timescales). It appears that the BRW would have to model anisotropy in each jump to account for the evolution in the SP distribution. Modeling the SP evolution with strain in polymers with different types of cross-links would be the next challenge in representing polymer network evolution using spatial branching processes.

Conflict of Interest

The authors declare no competing interests.

Acknowledgements

We thank Haotian Gu and Lenya Ryzhik for their helpful discussions. The material in this paper is based upon work supported by the Air Force Office of Scientific Research under award number FA9550-20-1-0397. Additional support is gratefully acknowledged from NSF 1915967, 2118199, 2229012, 2312204.

Data Availability

All details are available in the main text and the Supplementary appendices. The open source code for the branching random walk calculations along with the reference CGMD and theoretical predictions can be accessed from PolyBranchX.

References

[1] Fernando Carrillo, Shikha Gupta, Mehdi Balooch, Sally J Marshall, Grayson W Marshall, Lisa Pruitt, and Christian M Puttlitz. Nanoindentation of polydimethylsiloxane elastomers: Effect of crosslinking, work of adhesion, and fluid environment on elastic modulus. *Journal of Materials Research*, 20(10):2820–2830, 2005.

[2] B Erman and JE Mark. Rubber-like elasticity. *Annual Review of Physical Chemistry*, 40(1):351–374, 1989.

[3] Millard F Beatty. Topics in finite elasticity: Hyperelasticity of rubber, elastomers, and biological tissues—with examples. *Applied Mechanics Reviews*, 40:1699–1734, 1987.

[4] M Schiel, S Reh, M Schwienhorst, T Welters, E Stammen, and K Dilger. Finite element modelling of cure-dependent mechanical properties by model-free kinetic analysis using a cohesive zone approach. *The Journal of Adhesion*, 92(7-9):572–585, 2016.

[5] Mahdi Heydari-Meybodi, Saeed Saber-Samandari, and Mojtaba Sadighi. 3d multiscale modeling to predict the elastic modulus of polymer/nanoclay composites considering realistic interphase property. *Composite Interfaces*, 23(7):641–661, 2016.

[6] Ellen M Arruda and Mary C Boyce. A three-dimensional constitutive model for the large stretch behavior of rubber elastic materials. *Journal of the Mechanics and Physics of Solids*, 41(2):389–412, 1993.

[7] Kurt Kremer and Gary S Grest. Dynamics of entangled linear polymer melts: A molecular-dynamics simulation. *The Journal of Chemical Physics*, 92(8):5057–5086, 1990.

[8] Etienne Ducrot, Yulan Chen, Markus Bulters, Rint P Sijbesma, and Costantino Creton. Toughening elastomers with sacrificial bonds and watching them break. *Science*, 344(6180):186–189, 2014.

[9] Yikai Yin, Nicolas Bertin, Yanming Wang, Zhenan Bao, and Wei Cai. Topological origin of strain induced damage of multi-network elastomers by bond breaking. *Extreme Mechanics Letters*, 40:100883, 2020.

[10] Yikai Yin, Shaswat Mohanty, Christopher Cooper, Zhenan Bao, and Wei Cai. Network evolution controlling strain-induced damage and self-healing of elastomers with dynamic bonds. *In preparation*, 2023+.

[11] PJ Flory. Elasticity of polymer networks cross-linked in states of strain. *Transactions of the Faraday Society*, 56:722–743, 1960.

[12] Louigi Addario-Berry and Bruce Reed. Minima in branching random walks. *Annals of Probability*, 37(3):1044–1079, 2009.

[13] Elie Aïdékon. Convergence in law of the minimum of a branching random walk. *Annals of Probability*, 41(3A):1362–1426, 2013.

[14] Maury Bramson, Jian Ding, and Ofer Zeitouni. Convergence in law of the maximum of nonlattice branching random walk. *Annales de l'Institut Henri Poincaré - Probabilités et statistiques*, 52(4):1897–1924, 2016.

[15] Thomas Madaule. Convergence in law for the branching random walk seen from its tip. *Journal of Theoretical Probability*, 30:27–63, 2017.

[16] Maury D Bramson. Maximal displacement of branching Brownian motion. *Communications on Pure and Applied Mathematics*, 31(5):531–581, 1978.

[17] Steven P Lalley and Thomas Sellke. A conditional limit theorem for the frontier of a branching brownian motion. *The Annals of Probability*, pages 1052–1061, 1987.

[18] Matthew I Roberts. A simple path to asymptotics for the frontier of a branching Brownian motion. *Annals of Probability*, 41(5):3518–3541, 2013.

[19] Elie Aïdékon, Julien Berestycki, Éric Brunet, and Zhan Shi. Branching Brownian motion seen from its tip. *Probability Theory and Related Fields*, 157:405–451, 2013.

[20] Louis-Pierre Arguin, Anton Bovier, and Nicola Kistler. The extremal process of branching Brownian motion. *Probability Theory and related fields*, 157(3-4):535–574, 2013.

[21] Bastien Mallein. Maximal displacement in the d-dimensional branching Brownian motion. *Electronic Communications in Probability*, 20:1–12, 2015.

[22] Julien Berestycki, Yujin H Kim, Eyal Lubetzky, Bastien Mallein, and Ofer Zeitouni. The extremal point process of branching Brownian motion in $\mathbb{R}^d$. *arXiv preprint arXiv:2112.08407*, 2021.

[23] Yujin H Kim, Eyal Lubetzky, and Ofer Zeitouni. The maximum of branching Brownian motion in $\mathbb{R}^d$. *The Annals of Applied Probability*, 33(2):1515–1568, 2023.

[24] Viktor Bezborodov and Nina Gantert. The maximal displacement of radially symmetric branching random walk in $\mathbb{R}^d$. *arXiv preprint arXiv:2309.14738*, 2023.

[25] A. P. Thompson, H. M. Aktulga, R. Berger, D. S. Bolintineanu, W. M. Brown, P. S. Crozier, P. J. in 't Veld, A. Kohlmeyer, S. G. Moore, T. D. Nguyen, R. Shan, M. J. Stevens, J. Tranchida, C. Trott, and S. J. Plimpton. LAMMPS - a flexible simulation tool for particle-based materials modeling at the atomic, meso, and continuum scales. *Comp. Phys. Comm.*, 271:108171, 2022.

[26] Yelena R Sliozberg and Jan W Andzelm. Fast protocol for equilibration of entangled and branched polymer chains. *Chemical Physics Letters*, 523:139–143, 2012.

[27] Ting Ge, Flint Pierce, Dvora Perahia, Gary S Grest, and Mark O Robbins. Molecular dynamics simulations of polymer welding: Strength from interfacial entanglements. *Physical Review Letters*, 110(9):098301, 2013.

[28] Edsger W Dijkstra. A note on two problems in connexion with graphs. *Numerische Mathematik*, 1:269–271, 1959.

[29] Masao Doi, Samuel Frederick Edwards, and Samuel Frederick Edwards. *The Theory of Polymer Dynamics*, volume 73. Oxford University Press, 1988.

[30] William W Graessley. *Polymeric Liquids & Networks: Structure and Properties*. Garland Science, 2003.

[31] Christopher B Cooper, Jiheong Kang, Yikai Yin, Zhiao Yu, Hung-Chin Wu, Shayla Nikzad, Yuto Ochiai, Hongping Yan, Wei Cai, and Zhenan Bao. Multivalent assembly of flexible polymer chains into supramolecular nanofibers. *Journal of the American Chemical Society*, 142(39):16814–16824, 2020.

[32] Michael Rubinstein and Ralph H Colby. *Polymer Physics*, volume 23. Oxford University Press New York, 2003.

[33] Rolf Auhl, Ralf Everaers, Gary S Grest, Kurt Kremer, and Steven J Plimpton. Equilibration of long chain polymer melts in computer simulations. *The Journal of Chemical Physics*, 119(24):12718–12728, 2003.

[34] Michel Talagrand. A new look at independence. *Annals of Probability*, 24(1):1–34, 1996.

[35] Amir Dembo and Ofer Zeitouni. *Large Deviations Techniques and Applications*. Springer, 1998.

[36] Jose Blanchet, Wei Cai, Shaswat Mohanty, and Zhenyuan Zhang. On the first passage times of branching random walks in $\mathbb{R}^d$. *In preparation*, 2023+.

[37] Ronald Aylmer Fisher. The wave of advance of advantageous genes. *Annals of Eugenics*, 7(4):355–369, 1937.

[38] Andrei Kolmogorov, Petrovskii Ivan, and Piskunov Nikolai. Étude de l'équation de la diffusion avec croissance de la quantité de matière et son application à un problème biologigue. *Moscow Univ. Bull. Ser. Internat. Sect. A*, 1:1, 1937.

[39] Henry P McKean. Application of Brownian motion to the equation of Kolmogorov-Petrovskii-Piskunov. *Communications on Pure and Applied Mathematics*, 28(3): 323–331, 1975.

[40] Jürgen Gärtner. Location of wave fronts for the multi-dimensional K-P-P equation and Brownian first exit densities. *Mathematische Nachrichten*, 105(1):317–351, 1982.

[41] Arnaud Ducrot. On the large time behaviour of the multi-dimensional Fisher–KPP equation with compactly supported initial data. *Nonlinearity*, 28(4):1043, 2015.

[42] Jean-Michel Roquejoffre, Luca Rossi, and Violaine Roussier-Michon. Sharp large time behaviour in N-dimensional Fisher-KPP equations. *Discrete and Continuous Dynamical Systems A*, 39:7265–7290, 2019.

[43] Mehmet Öz. On the density of branching Brownian motion. *Hacettepe Journal of Mathematics & Statistics*, 52(1):229–247, 2023.

[44] Ali Fuat Yeniçerioğlu, Vildan Yazıcı, and Cüneyt Yazıcı. Asymptotic behavior and stability in linear impulsive delay differential equations with periodic coefficients. *Mathematics*, 8(10):1802, 2020.

Appendix A. Proofs of results in Section 4

Appendix A.1. Proof of Theorem 1 and related discussions

In this appendix, we prove Theorem 1. Let us first summarize a few preliminary results from the literature. In the following, we work in a general dimension $d \geqslant 1$ and assume the BBM is standard. Denote by M_t the maximal displacement of the BBM at time t. The first precise asymptotic in dimension $d = 1$ for M_t was given by [16], whose proof was later considerably simplified by [18]. More precisely, we have

$$M_t = \sqrt{2}\, t - \frac{3}{2\sqrt{2}} \log t + O_{\mathbb{P}}(1). \tag{A.1}$$

Finer behavior near the frontier was analyzed by [19] and [20]. In dimension $d > 1$, we mention the very recent works of [23] and [22] on characterizing the behavior of the maximal norm of the BBM in $\mathbb{R}^d$, where the precise asymptotic was first given by [21].

The BBM is intimately connected to the *Fisher-KPP equation* introduced by [37, 38]—it is shown by [39] that $v(t, x) = \mathbb{P}(M_t > x)$ solves the Fisher-KPP initial value problem $v_t = v_{xx}/2 + v - v^2$, with initial condition $v(0, x) = \mathbb{1}_{\{x \leqslant 0\}}$. Analogously, as pointed out by [21], in dimension $d \geqslant 1$, $v(t, x) = \mathbb{P}(\exists u \in \mathcal{N}_t : \|X_t(u) - \mathbf{x}\| \leqslant 1)$ solves the multi-dimensional Fisher-KPP equation

$$\begin{cases} v_t = \frac{1}{2}\Delta v + v - v^2, \ t > 0, \ \mathbf{x} \in \mathbb{R}^d, \\ v(0, \mathbf{x}) = \mathbb{1}_{\{\mathbf{x} \in B_{\mathbf{0}}(1)\}}. \end{cases} \tag{A.2}$$

Here and later, we let $\mathcal{N}_t$ be the collection of particles at time t and $X_t(u)$ the location of a particle $u \in \mathcal{N}_t$ at time t. The multi-dimensional Fisher-KPP equation has been studied by [40] in a probabilistic framework and later by [41] and [42] using a PDE approach, where it is shown that the level set $v = 1/2$ appears at $x = \sqrt{2}t - ((d+2)\log t)/(2\sqrt{2}) + O_{\mathbb{P}}(1)$.[19] Consequently, [21] stated that "the probability to find an individual within distance 1 of a given point $\mathbf{x}$ is small if $\|\mathbf{x}\| \gg \sqrt{2}t - ((d+2)\log t)/(2\sqrt{2})$ and large if $\|\mathbf{x}\| \ll \sqrt{2}t - ((d+2)\log t)/(2\sqrt{2})$." Formally, with $A(x) = x/\sqrt{2} + ((d+2)\log x)/4$, the following result holds.

Theorem 4. *Fix $\varepsilon > 0$. There exists $C = C(\varepsilon) > 0$ such that for every $\mathbf{x} \in \mathbb{R}^d$ with $\|\mathbf{x}\|$ large enough and every $t < A(\|\mathbf{x}\|) - C$,*

$$\mathbb{P}(\exists u \in \mathcal{N}_t : \|X_t(u) - \mathbf{x}\| \leqslant 1) < \varepsilon,$$

and for every $t > A(\|\mathbf{x}\|) + C$,

$$\mathbb{P}(\exists u \in \mathcal{N}_t : \|X_t(u) - \mathbf{x}\| \leqslant 1) > 1 - \varepsilon.$$

[19] Inverting this relation gives $t = x/\sqrt{2} + ((d+2)\log x)/4 + O_{\mathbb{P}}(1)$, giving precisely (5).

Remark 1. In a similar manner, finding the FPT for a domain in $\mathbb{R}^d$ is equivalent to solving the multi-dimensional Fisher-KPP equation with a Dirichlet boundary condition; see e.g., the derivation in [39] and the Appendix of [16]. More precisely, consider the boundary value problem

$$\begin{cases} v_t = \frac{1}{2}\Delta v + v - v^2, \ t > 0, \ \mathbf{x} \in \mathbb{R}^d, \\ v(0, \mathbf{x}) = \mathbb{1}_{\{\mathbf{x} \in B_{\mathbf{0}}(1)\}}, \\ v(t, \mathbf{x}) = 1, \ t > 0, \ \mathbf{x} \in \mathbb{S}^{d-1}. \end{cases} \tag{A.3}$$

It holds that $v(t, \mathbf{x}) = \mathbb{P}(\tau_{\mathbf{x}} < t)$, the probability that the BBM starting from $\mathbf{0} \in \mathbb{R}^d$ has already reached $B_{\mathbf{x}}(1)$ by time t. Nevertheless, we are not aware of studies of (A.3), given that it is a boundary value problem instead of an initial value problem. Our Theorem 1 shows that asymptotically, the solutions to the two problems (A.2) and (A.3) are reasonably close.

Proof of Theorem 1. The upper bound of τ_x follows directly from Theorem 4. For the lower bound, we fix $\varepsilon > 0$ and an increasing sequence $a(x) \to \infty$, and it suffices to show for x large enough,

$$\mathbb{P}\left(\tau_x \leqslant \frac{x}{\sqrt{2}} + \frac{d+2}{4}\log x - a(x)\right) < \varepsilon. \tag{A.4}$$

Observe that with $\mathbf{x} = (x, 0 \ldots, 0) \in \mathbb{R}^d$ and $t_0 = x/\sqrt{2} + ((d+2)\log x)/4 - a(x)/2$,

$$\begin{aligned} &\mathbb{P}\left(\tau_x \leqslant \frac{x}{\sqrt{2}} + \frac{d+2}{4}\log x - a(x)\right) \\ &\leqslant \mathbb{P}(\exists u \in \mathcal{N}_{t_0} : \|X_{t_0}(u) - \mathbf{x}\| \leqslant 3) + \mathbb{P}(\forall u \in \mathcal{N}_{t_0-\tau_x} : \|X_{t_0-\tau_x}(u)\| \geqslant 2; \tau_x \leqslant t_0 - \frac{a(x)}{2}). \end{aligned}$$

Since a ball of radius 3 can be covered by finitely many balls of radius 1 in $\mathbb{R}^d$, the first probability is bounded by $\varepsilon/2$ for x large. Splitting the second probability on the events $\tau_x \in (j-1, j]$ we obtain

$$\begin{aligned} &\mathbb{P}\left(\forall u \in \mathcal{N}_{t_0-\tau_x} : \|X_{t_0-\tau_x}(u)\| \geqslant 2; \tau_x \leqslant t_0 - \frac{a(x)}{2}\right) \\ &\qquad \leqslant \sum_{j=1}^{\infty} \mathbb{P}\left(\exists t \in \left(\frac{a(x)}{2} + j - 1, \frac{a(x)}{2} + j\right), \ \forall u \in \mathcal{N}_t, \ \|X_t(u)\| \geqslant 2\right). \end{aligned}$$

Divide equally the interval $(a(x)/2 + j - 1, a(x)/2 + j)$ into $q_x(j) := \exp((a(x)/2 + j)/3)$ many intervals $\{I_\ell\}$ with endpoints $a(x)/2 + j - 1 = t_0 < \cdots < t_{q_x(j)} = a(x)/2 + j$. Denote by $\mathbf{Z}$ a d-dimensional standard Gaussian random variable and write $u \mapsto v$ if v

is a descendant of u. We have

$$\begin{aligned}
&\mathbb{P}\left(\exists t \in \left(\frac{a(x)}{2}+j-1, \frac{a(x)}{2}+j\right),\ \forall u \in \mathcal{N}_t,\ \|X_t(u)\| \geqslant 2\right) \\
&\leqslant \sum_{\ell=1}^{q_x(j)} \mathbb{P}(\forall u \in \mathcal{N}_{t_\ell},\ \|X_{t_\ell}(u)\| \geqslant 1) + \mathbb{P}\left(\sup_{\ell} \sup_{\substack{s,t \in I_\ell \\ s>t}} \sup_{\substack{u \in \mathcal{N}_t, v \in \mathcal{N}_s \\ u \mapsto v}} \|X_t(u) - X_s(v)\| \geqslant 1\right) \\
&\leqslant \sum_{\ell=1}^{q_x(j)} \mathbb{P}(\forall u \in \mathcal{N}_{t_\ell},\ \|X_{t_\ell}(u)\| \geqslant 1) + q_x(j) e^{2(a(x)/2+j)} \mathbb{P}\left(\|\mathbf{Z}\| \geqslant \sqrt{q_x(j)}\right) + o(1) \\
&= \sum_{\ell=1}^{q_x(j)} \mathbb{P}(\forall u \in \mathcal{N}_{t_\ell},\ \|X_{t_\ell}(u)\| \geqslant 1) + o(1),
\end{aligned}$$

where in the second inequality we used Markov's inequality on the number of particles present at time $a(x)/2 + j$. By Theorem 2.1 of [43] applied with $a = k = \theta = 0$ and $r_0 = 1$, for x large,

$$\mathbb{P}(\forall u \in \mathcal{N}_{t_\ell},\ \|X_{t_\ell}(u)\| \geqslant 1) \leqslant e^{-(a(x)/2+j-1)/2}.$$

Altogether, we obtain the bound (A.4). □

Appendix A.2. Proof of the remaining results from Section 4

Proof of Corollary 2. Fix a dimension $d \geqslant 1$, and let us denote by $\tau^r_{\kappa,s}(x)$ the FPT of a BBM with branching rate κ and diffusivity s to a ball of radius r centered at $(x, 0, \dots, 0) \in \mathbb{R}^d$. In particular, $\tau^1_{\kappa,s}(x) = \tau_{\kappa,s}(x)$. By self-similarity of the Brownian motion, we have the relations

$$\tau^1_{\kappa,s}(x) \overset{\text{law}}{=} \tau^{s^{-1}}_{\kappa,1}\left(\frac{x}{s}\right) \qquad \text{and} \qquad \tau^1_{\kappa,s}(x) \overset{\text{law}}{=} \frac{1}{\kappa}\tau^{\sqrt{\kappa}}_{1,s}\left(\sqrt{\kappa}x\right)$$

for every $\kappa, s > 0$. The proof then follows immediately from Theorem 1, where we note that the same proof works if we replace the target B_x by a ball centered at $(x, 0, \dots, 0) \in \mathbb{R}^d$ of a fixed radius $r > 0$. □

Proof of Theorem 3. Note that the only difference between the classical BRW and our delayed branching BRW models is the branching structure, i.e., the underlying tree that describes the genealogy of the particles. The proof of the version of Theorem 3 for classical BRW depends on the branching structure only through the first moment and second moment estimates; see (28) and (29) of [14]. In our case, this can be adapted using Lemma 5 below. □

Lemma 5. *Conditioned upon survival, the expected number of particles N_n at time n for the delayed branching BRW model satisfies $N_n \asymp \rho^n$,[20] where ρ is given by (10).*

[20]For two sequences $\{A_n\}$ and $\{B_n\}$, we write $A_n \asymp B_n$ if there is a constant $C > 0$ independent of n such that $A_n/C \leqslant B_n \leqslant CA_n$ for all n.

Proof. Let us first prove that $\widetilde{N}_n \asymp \rho^n$ where $\widetilde{N}_n$ is the expected value of Z_n, the number of particles at time n (without conditioning upon survival). Recall from Section 2.4 that in the delayed branching regime, each branching event consists of two branching sub-events at consecutive times, both into two branches. We call the first of the two sub-events the *branching of type I*, and the second *branching of type II*. For $n \in \mathbb{N}$, let α_n be the expected number of branching sub-events of type I at time $n-1$. By construction, this is the same expected number of branching sub-events of type II at time n. Our definition of the delayed branching regime then leads to the following recursive equations of $(\widetilde{N}_n, \alpha_n)$:

- $\widetilde{N}_1 = 1,\ \alpha_1 = 0$;
- each particle at time n that does not initiate a branching of type II independently has probability $\widetilde{\kappa}$ to create a branching of type I, thus $\alpha_{n+1} = \widetilde{\kappa}(\widetilde{N}_n - \alpha_n)$;
- the increment of particles at time $n+1$ comes from contributions from branchings of types both I and II, meaning that $\widetilde{N}_{n+1} = 2(1-\widetilde{\nu})\alpha_n + (1+\widetilde{\kappa}-\widetilde{\nu})(\widetilde{N}_n - \alpha_n)$.

In matrix form, we write

$$\begin{aligned}\begin{bmatrix}\widetilde{N}_{n+1}\\ \alpha_{n+1}\end{bmatrix} &= \begin{bmatrix}1+\widetilde{\kappa}-\widetilde{\nu} & 1-\widetilde{\kappa}-\widetilde{\nu}\\ \widetilde{\kappa} & -\widetilde{\kappa}\end{bmatrix}\begin{bmatrix}\widetilde{N}_n\\ \alpha_n\end{bmatrix}\\ &= \begin{bmatrix}1+\widetilde{\kappa}-\widetilde{\nu} & 1-\widetilde{\kappa}-\widetilde{\nu}\\ \widetilde{\kappa} & -\widetilde{\kappa}\end{bmatrix}^n\begin{bmatrix}1\\ 0\end{bmatrix} =: M(\widetilde{\kappa},\widetilde{\nu})^n\begin{bmatrix}1\\ 0\end{bmatrix}.\end{aligned}$$

The largest eigenvalue of the matrix $M(\widetilde{\kappa},\widetilde{\nu})$ is precisely $\rho(\widetilde{\kappa},\widetilde{\nu})$ defined in (10), and we conclude that $\widetilde{N}_n \asymp \rho^n$.

Denote by $p = 1-q = \mathbb{P}(S)$. We first prove that $q < 1$ if $\rho > 1$. Let $q_n = \mathbb{P}(Z_n = 0)$, so that $q_n \uparrow q$. By construction of the delayed branching regime, we have $q_1 = \widetilde{\nu}$, $q_2 = \widetilde{\nu} + (1-\widetilde{\kappa}-\widetilde{\nu})q_1 + \widetilde{\kappa}\widetilde{\nu}^2 q_1$, and for $n \geqslant 1$,

$$q_{n+2} = \widetilde{\nu} + (1-\widetilde{\kappa}-\widetilde{\nu})q_{n+1} + \widetilde{\kappa}(1-\widetilde{\nu})^2 q_{n+1}q_n^2 + \widetilde{\kappa}\widetilde{\nu}^2 q_{n+1} + 2\widetilde{\kappa}\widetilde{\nu}(1-\widetilde{\nu})q_{n+1}q_n. \quad \text{(A.5)}$$

Consider the equation

$$q = h(q) := \widetilde{\nu} + (1-\widetilde{\kappa}-\widetilde{\nu})q + \widetilde{\kappa}(1-\widetilde{\nu})^2 q^3 + \widetilde{\kappa}\widetilde{\nu}^2 q + 2\widetilde{\kappa}\widetilde{\nu}(1-\widetilde{\nu})q^2.$$

It is elementary to check that $h(0) = \widetilde{\nu} \geqslant 0$, $h(1) = 1$, and that if $\rho > 1$, then $h'(1) < 1$. In particular, there exists a solution $\hat{q} \in (\widetilde{\nu}, 1)$ to the equation $q = h(q)$. It follows from (A.5) that if $q_n \leqslant q_{n+1} \leqslant \hat{q}$, then $q_{n+2} \leqslant \hat{q}$. By induction, we know that $q_n \leqslant \hat{q}$ for each n. Therefore, $q = \lim q_n \leqslant \hat{q} < 1$.

Observe that $\widetilde{N}_n = pN_n + q\mathbb{E}[Z_n \mid S^c]$. Since we have the bound

$$\mathbb{P}(Z_n > y \mid S^c) = \frac{\mathbb{P}(Z_n > y,\, S^c)}{q} \leqslant \frac{\mathbb{P}(S^c \mid Z_n > y)}{q} \leqslant q^{y-1},$$

it holds $\mathbb{E}[Z_n \mid S^c] \leqslant C(q)$. Hence, we conclude that $N_n \asymp \rho^n$. □

Appendix B. Numerical validation of the first passage time asymptotics

In this appendix, we provide numerical verification of the FPT asymptotics for BRW (13) and BBM (6). In particular, we show that the path purging in our numerical algorithm affects very little the FPT.

Appendix B.1. Validation of the asymptotic (13)

Recall that the coefficient $1/c_1$ of the linear term for the estimation (13) of τ_x can be computed through the relation $I(c_1) = \log \rho$. Recall also that $\widetilde{\nu} = 2/l_c$ is the termination rate and

$$\rho = \rho(\widetilde{\kappa}, \widetilde{\nu}) = \frac{1-\widetilde{\nu}}{2} + \sqrt{\frac{(1-\widetilde{\nu})^2}{4} + 2\widetilde{\kappa}(1-\widetilde{\nu})}.$$

The implicit relation between c_1 and $\widetilde{\kappa}$ can thus be computed for the BRW and compared against the numerical BRW implementation.

Next, we compute numerically the relation between c_1 and $\widetilde{\kappa}$. For any given $\widetilde{\kappa}$, we calculate the SP distribution for 1000 paths at different offset distances for $q_x \in [20, 60]$. The mean SP (same as the FPT for a unit length jump per unit time), $\tau(q_x)$, is then fit to a function of the form,

$$\tau(q_x) = \frac{q_x}{c_1} + B\log(q_x) + C. \tag{B.1}$$

The parameter $\widetilde{\kappa}$ is obtained by uniformly sampling 19 points from $[0.05, 0.95]$.

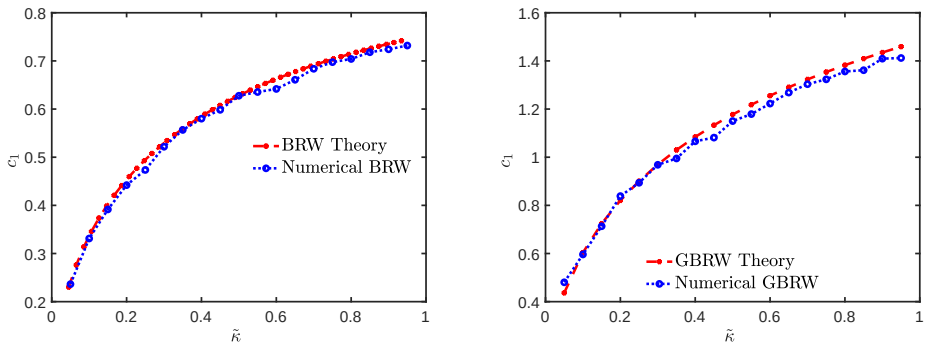

(a) (b)

Figure B.14: The numerical BRW obtained c_1 compared against the reference calculation (13) at different branching rate $\widetilde{\kappa}$ for the BRW model with increments (a) uniformly distributed on $\mathbb{S}^2$ (BRW); (b) Gaussian distributed on $\mathbb{R}^3$ (GBRW).

We see that the numerically obtained coefficient c_1 of the linear term is in decent agreement with the reference theory estimates for the BRW, as shown in Figure B.14. This indicates that the numerical approximation of path purging does not affect the linear coefficient of the scaling behavior of the SP or FPT distribution of the numerical BRW, and can be used as a suitable approximation for carrying out the numerical BRW to represent a CGMD network.

Appendix B.2. Validation of the asymptotic (6)

We use a similar approach to verify the theoretical prediction (6) for the FPT of the standard BBM. Note that here we do not include the termination or delayed branching regimes. With the choice of $\sigma = 1$, the coefficient $1/c_1$ for (6) is equal to $1/\sqrt{2\widetilde{\kappa}}$ for $\widetilde{\kappa} > 0$.

For $\widetilde{\kappa}$ sampled uniformly in $[0.05, 0.95]$, we compute numerically the mean first passage times $\tau(q_x)$ at different offset distances $q_x \in [20, 60]$ and fit them to a function of the form (B.1). The linear coefficient demonstrates a decent agreement with the theoretical prediction, as shown in Figure B.15. Again, this supports that path purging

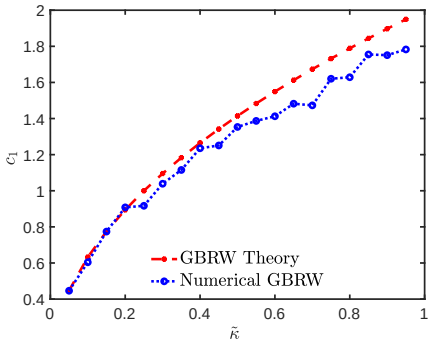

Figure B.15: The c_1 obtained numerically from the BBM compared against the theoretical estimate at different branching rates $\widetilde{\kappa}$ for the BRW model.

has a negligible effect on the distribution of the FPT. The divergence of the behavior of the numerical implementation from the theoretical estimate occurs due to the pseudo-continuous implementation of time (discrete time steps of 0.1). The effect of discretization is negligible at lower branching rates (even with a time step of 0.25 for $\widetilde{\kappa} \leqslant 0.1$), but becomes more apparent for $\widetilde{\kappa} > 0.3$ which is well above the cross-link density in realistic polymeric systems that are simulated using the CGMD method.

Appendix C. Intercept of the linear dependency

We have used *linear dependency*, $\overline{c}_1$, to classify the quality of agreement of the numerical model to the CGMD calculations, as shown in Figures 6(a), 9(a) and 12(a). However, the same linear dependency $\overline{c}_1$ may represent a family of straight lines with a slope of $1/\overline{c}_1$ but distinct intercepts. As a result, to fully characterize the SP mean we look at the *intercept*, $\mathrm{SP}(q_x = 0)$. We see that the three presented numerical models are in agreement with the CGMD results, barring at lower cross-link densities as shown in Figure C.16.

Appendix D. Shortest path in the 8-chain model

In this appendix, we present the comparison of the theoretical estimates of $\overline{c}_1$ obtained from the spatial branching processes (scaled BRW, GBRW, and BBM). The intuition is that the idealized and simplified 8-chain (a.k.a. Arruda-Boyce) model places

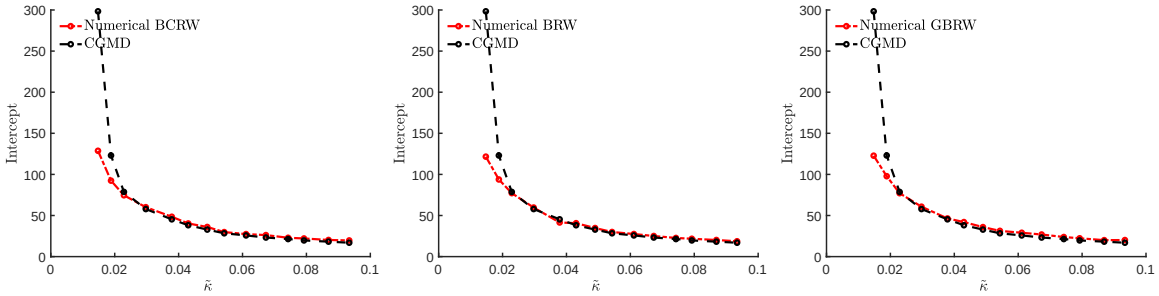

(a) (b) (c)

Figure C.16: The intercepts of the SP(q_x) for the (a) BCRW, (b) scaled BRW, and (c) scaled GBRW methods.

all chains along the shortest path. This makes the shortest path between distance nodes much longer than the spatial branching models, for the realistic range of branching rates encountered in the CGMD simulations ($\widetilde{\kappa} < 0.1$). The resultant $\overline{c}_1$ is expected to be

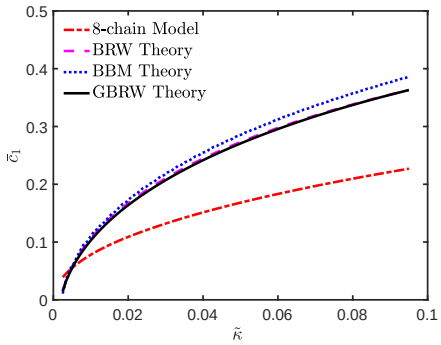

Figure D.17: The $\overline{c}_1$ computed analytically from the theoretical estimate at different branching rates $\widetilde{\kappa}$ for the 8-chain, scaled BRW, GBRW, and BBM models. The scaling of the jumps as a function of the MSID has been accounted for resulting in an additional $1/\sigma$ factor multiplying the estimates in (7) and (14).

much lower in the 8-chain model as a consequence and this is confirmed by the theoretical estimate of $\overline{c}_1$ from the 8-chain model and the other spatial branching processes, as shown in Figure D.17.

Appendix E. Approximating GBRW with BBM

In this appendix, we discuss how to approximate our GBRW model (see Section 3.3 for details) by a standard BBM with an implied branching rate. Recall from Section 2.4 that we introduced the extra features of termination and delayed branching property. The analogies for the BBM can be summarized as follows:

- termination: each existent particle carries an independent exponential clock with rate $\widetilde{\nu} = 1/250$, representing the termination of the particle;

- delayed branching property: the branching events occur according to exponential clocks with parameter $\widetilde{\kappa}$. Each branching event consists of two sub-events: the particle first branches into two and then one of the two descendants branches into two after a unit of time (within this unit of time, termination could happen but no extra branching event will occur).

The resulting model will be called the $(\widetilde{\kappa},\widetilde{\nu})$-BBM. Unfortunately, both the termination and the delayed branching properties are not handy to deal with when analyzing the FPT, due to the reminiscence of the connection to Fisher-KPP equations. Nevertheless, we still expect that a correspondent asymptotic result of the form (13) with an $O_{\mathbb{P}}(\log\log x)$ error term should at least hold true.

For clarity of our discussions, we take the following detour. It is not unreasonable to approximate the $(\widetilde{\kappa},\widetilde{\nu})$-BBM model (conditioned upon non-extinction) with the classical BBM model that carries the same asymptote for the expected number of particles. Consider the $(\widetilde{\kappa},\widetilde{\nu})$-BBM where $2\widetilde{\kappa}>\widetilde{\nu}$, and denote by $n(t):=\mathbb{E}[\#\mathcal{N}_t]$, the expected number of particles at time t.

Proposition 6. *Denote by $\lambda_0>0$ the unique real root to $\lambda_0=-\widetilde{\nu}+2\widetilde{\kappa}e^{-\lambda_0}$. It holds that $n(t)\asymp e^{\lambda_0 t}$.*

Proof. By our construction, and conditioning on the first branching/termination event, there is

$$\begin{aligned} n(t) = e^{-t(\widetilde{\kappa}+\widetilde{\nu})} &+ \int_0^t \widetilde{\kappa}\, e^{-(\widetilde{\kappa}+\widetilde{\nu})s} n(t-s)\mathrm{d}s \\ &+ 2\int_0^t \widetilde{\kappa}\, e^{-(\widetilde{\kappa}+\widetilde{\nu})s}\left(n(t-s-1)\mathbb{1}_{\{s\leqslant t-1\}}+\mathbb{1}_{\{t-1<s\leqslant t\}}\right)\mathrm{d}s. \end{aligned}$$

Duhamel's principle then yields the delay differential equation

$$n'(t) = -\widetilde{\nu}\, n(t) + 2\widetilde{\kappa}\left(n(t-1)\mathbb{1}_{\{t\geqslant 1\}}+\mathbb{1}_{\{0\leqslant t<1\}}\right). \tag{E.1}$$

Let us introduce the solution $\phi(t)=\mathbb{E}[\#\mathcal{N}_t]$ for $0\leqslant t\leqslant 1$, where $1\leqslant\phi(t)\leqslant C(\widetilde{\kappa})$ for some $C(\widetilde{\kappa})>0$. The solution to (E.1) then satisfies the linear autonomous impulsive delay differential equation

$$n'(t) = -\widetilde{\nu}\, n(t) + 2\widetilde{\kappa}\, n(t-1),\ n|_{[0,1]}=\phi|_{[0,1]}. \tag{E.2}$$

Recall our definition of λ_0, which is the root of the characteristic equation associated with (E.2). That $\lambda_0>0$ follows from $2\widetilde{\kappa}>\widetilde{\nu}$. Theorem 1 of [44] then leads to $\lim_{t\to\infty} n(t)e^{-\lambda_0 t}=C(\phi)$ for some constant $C(\phi)$ depending on ϕ that is uniformly bounded when $\widetilde{\kappa}\leqslant 1$. In other words, $n(t)\asymp e^{\lambda_0 t}$. □

Upon solving for λ_0, the $(\widetilde{\kappa},\widetilde{\nu})$-BBM can be approximated by a scaled BBM with binary branching and implied branching rate λ_0. The diffusivity of the BBM is now set to $s=\sqrt{\mathrm{MSID}(1/\widetilde{\kappa})/3}$ in view of the central limit theorem. This explains the regime behind the *BBM Theory* curve in Figure 12(a).